Deep Learning in CT Artifact Correction

Marc Kachelrieß

German Cancer Research Center (DKFZ)
Heidelberg, Germany
www.dkfz.de/ct

Content

- Metal artifact reduction (MAR)
- Ring artifact reduction (RAR)
- Detruncation
- Scatter estimation
- Motion compensation
- Sparse view artifacts
- Limited angle artifacts

Deep MAR Examples

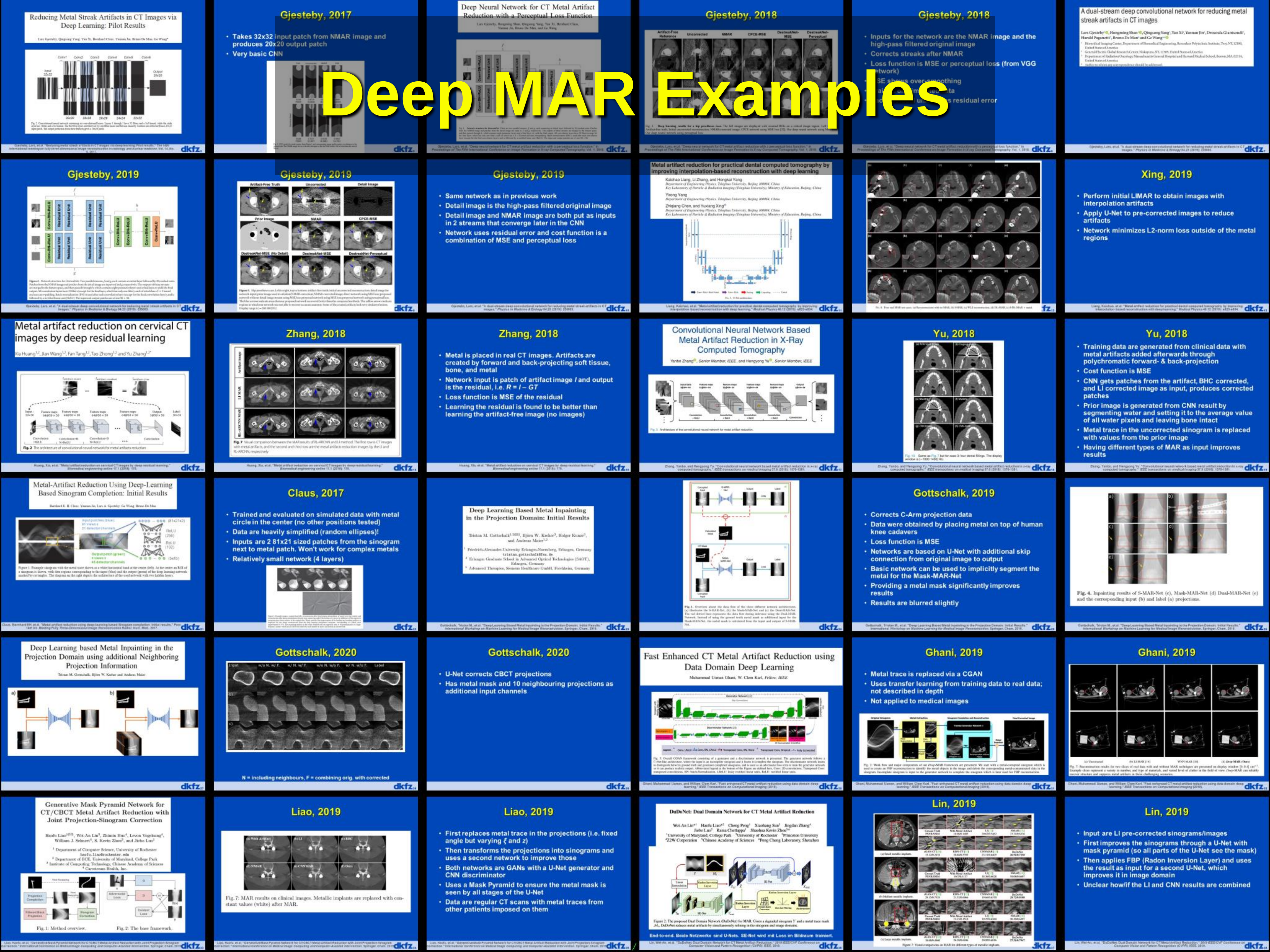

Metal artifacts are

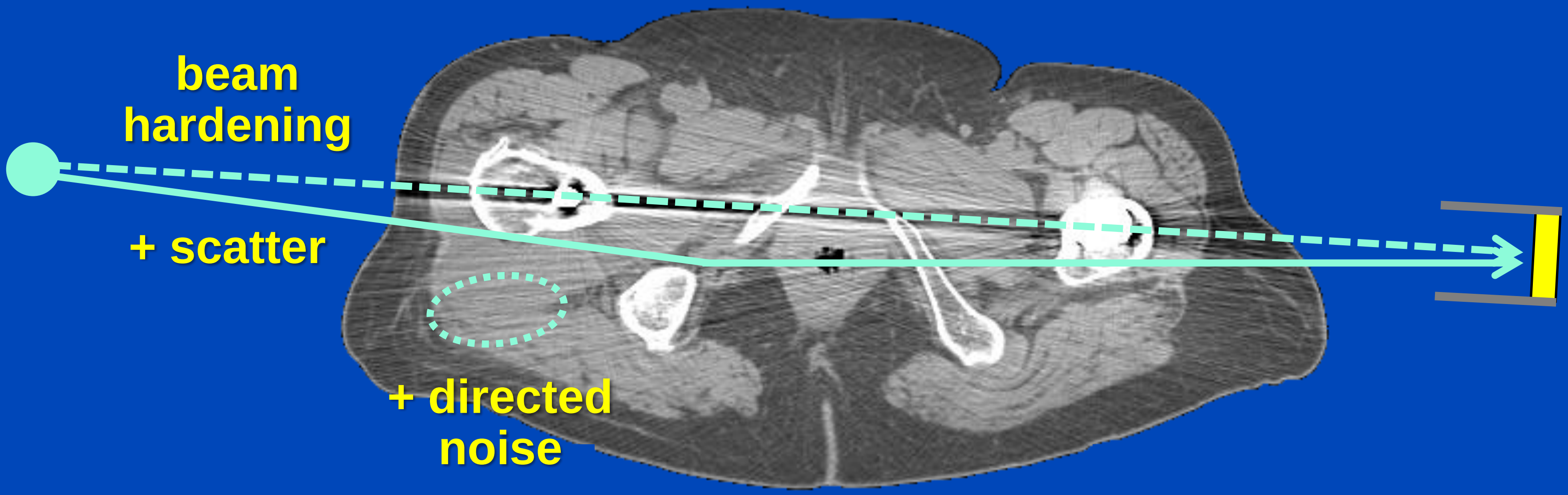

+ increased susceptibility to sampling artifacts and motion.

MAR Example

- Deep CNN-driven patch-based combination of the advantages of several MAR methods trained on simulated artifacts

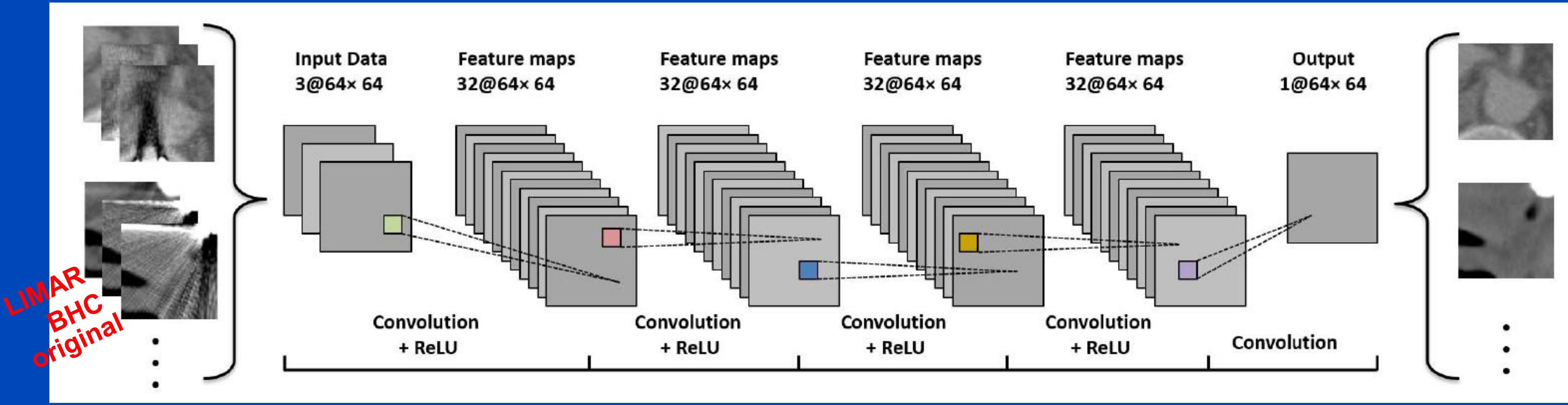

- followed by segmentation into tissue classes
- followed by forward projection of the CNN prior and replacement of metal areas of the original sinogram
- followed by reconstruction

Yanbo Zhang and Hengyong Yu. Convolutional Neural Network Based Metal Artifact Reduction in X-Ray Computed Tomography. TMI 37(6):1370-1381, June 2018.

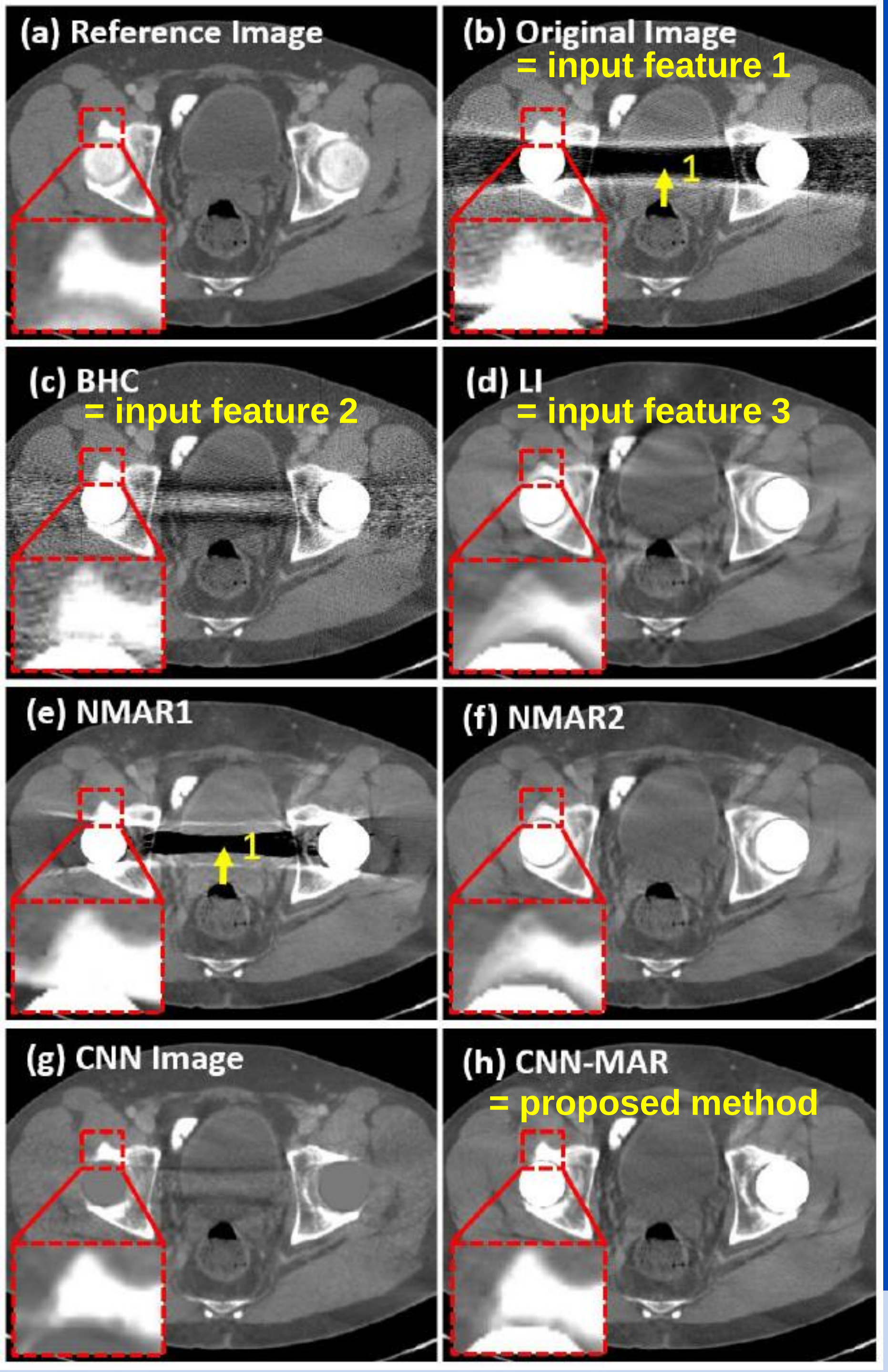
(a) Reference Image
(b) Original Image
= input feature 1
1
(c) BHC
= input feature 2
(d) LI
= input feature 3
(e) NMAR1
1
(f) NMAR2
(g) CNN Image
(h) CNN-MAR
= proposed method

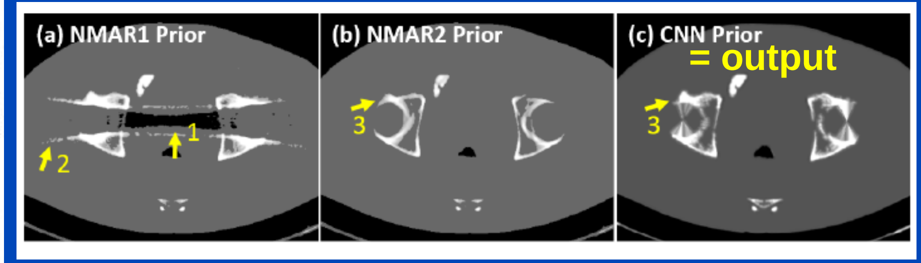
(a) NMAR1 Prior
1
2
(b) NMAR2 Prior
3
(c) CNN Prior
= output
3

Metal artifact reduction for practical dental computed tomography by improving interpolation-based reconstruction with deep learning

Kaichao Liang, Li Zhang, and Hongkai Yang
Department of Engineering Physics, Tsinghua University, Beijing 100084, China
Key Laboratory of Particle & Radiation Imaging (Tsinghua University), Ministry of Education, Beijing, China

Yirong Yang
Department of Engineering Physics, Tsinghua University, Beijing 100084, China

Zhiqiang Chen, and Yuxiang Xing[a)]
Department of Engineering Physics, Tsinghua University, Beijing 100084, China
Key Laboratory of Particle & Radiation Imaging (Tsinghua University), Ministry of Education, Beijing, China

LI-MAR image in

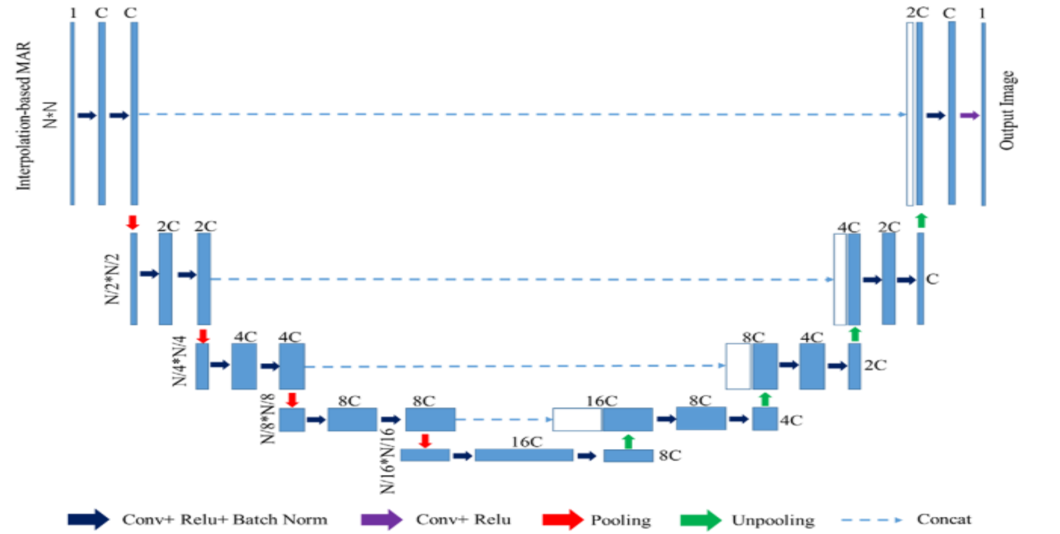

FIG. 3. U-Net architecture.

nicer image out

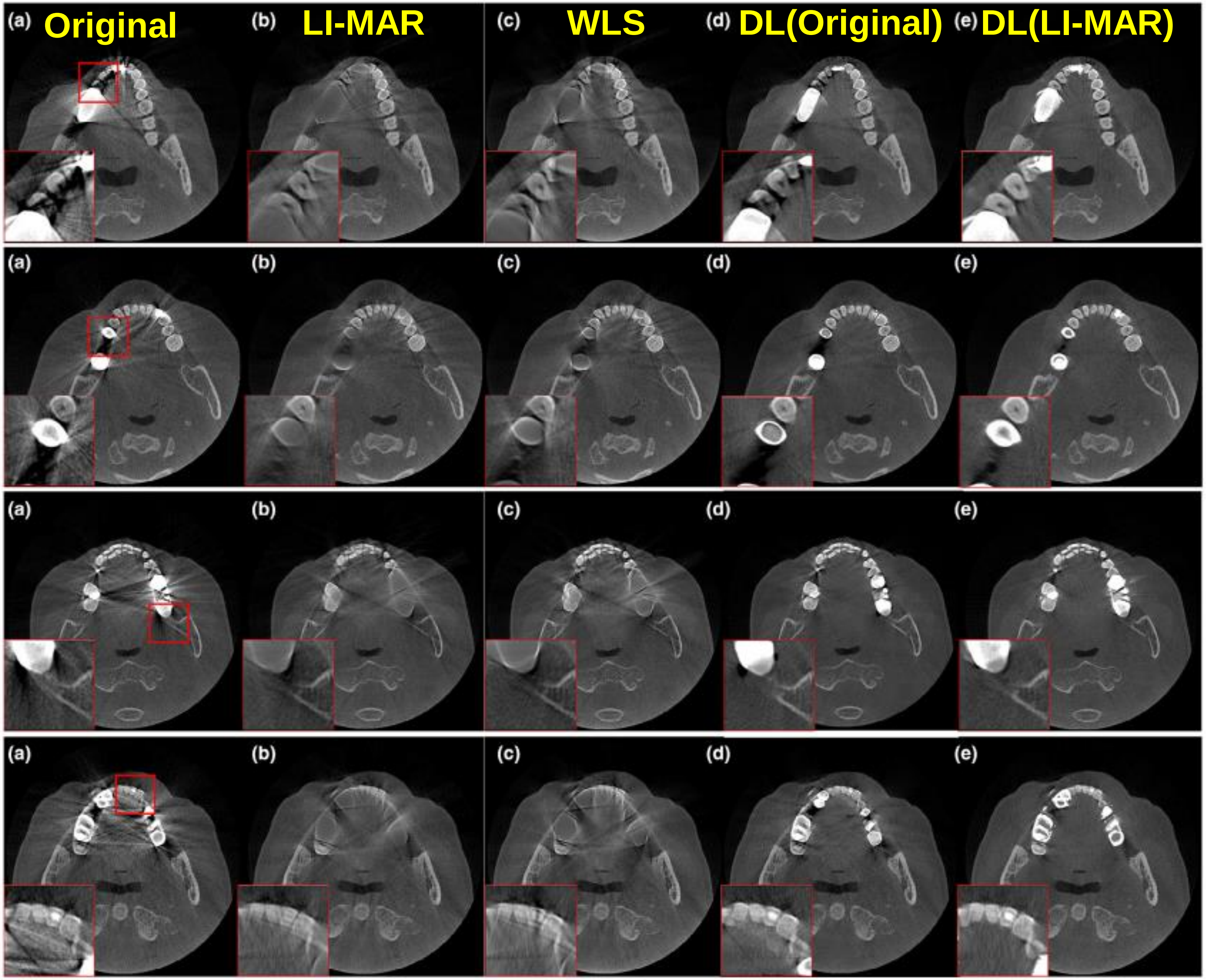

FIG. 8. Four real MAR test cases. (a) Reconstructions with no MAR, (b) I-MAR, (c) WLS reconstruction, (d) DL-MAR, (e) I-DL-MAR + metal.

MAR without Machine Learning is a Good Alternative: Frequency Split Normalized MAR[1,2]

Uncorrected FSLIMAR FSNMAR

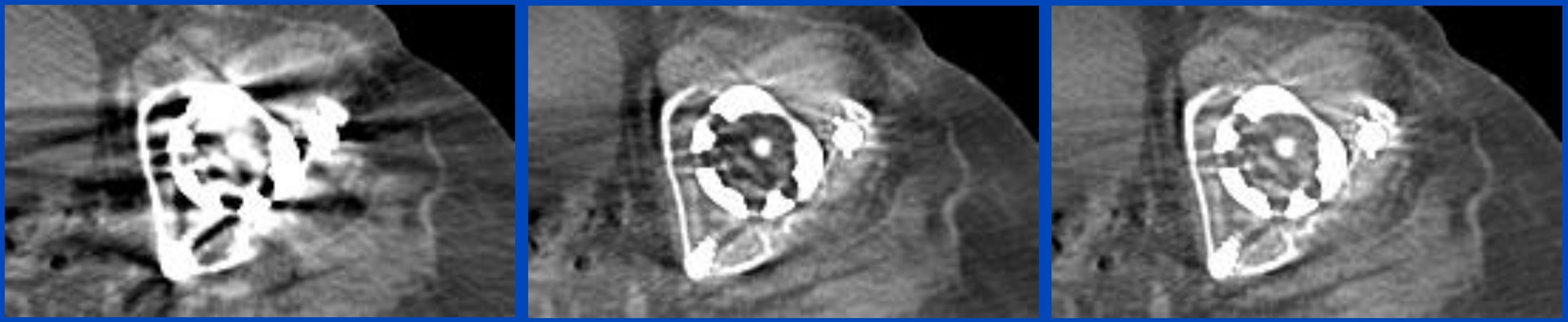

Patient with bilateral hip prosthesis, Somatom Definition Flash, (C=40/W=500).

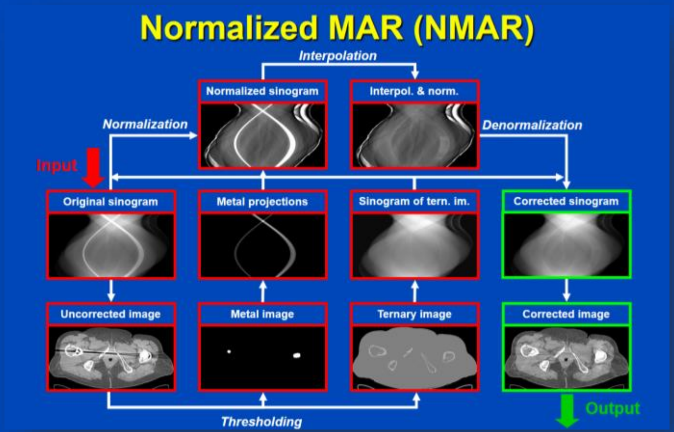

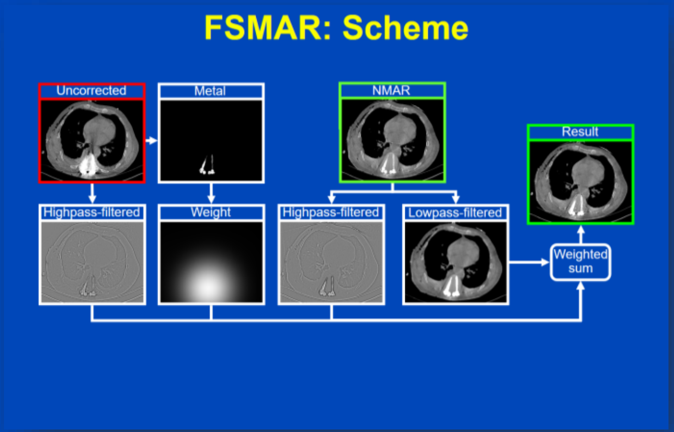

[1]E. Meyer, M. Kachelrieß. Normalized metal artifact reduction (NMAR) in computed tomography. Med. Phys. 37(10):5482-5493, Oct. 2010.
[2]E. Meyer, M. Kachelrieß. Frequency split metal artifact reduction (FSMAR) in CT. Med. Phys. 39(4):1904-1916, April 2012.

Summary on Deep MAR

- **Most common uses for networks:**
  - Improve image quality in image domain after MAR
  - Use network for the sinogram inpainting
  - Produce a prior image, e.g. for NMAR
- **Additional observations:**
  - Training data are often produced by segmenting an artifact-free CT image, adding metal and applying a polychromatic forward projection to different types of tissue separately.
  - As of today, it seems hard to outperform NMAR, or hard to give convincing clinical examples.

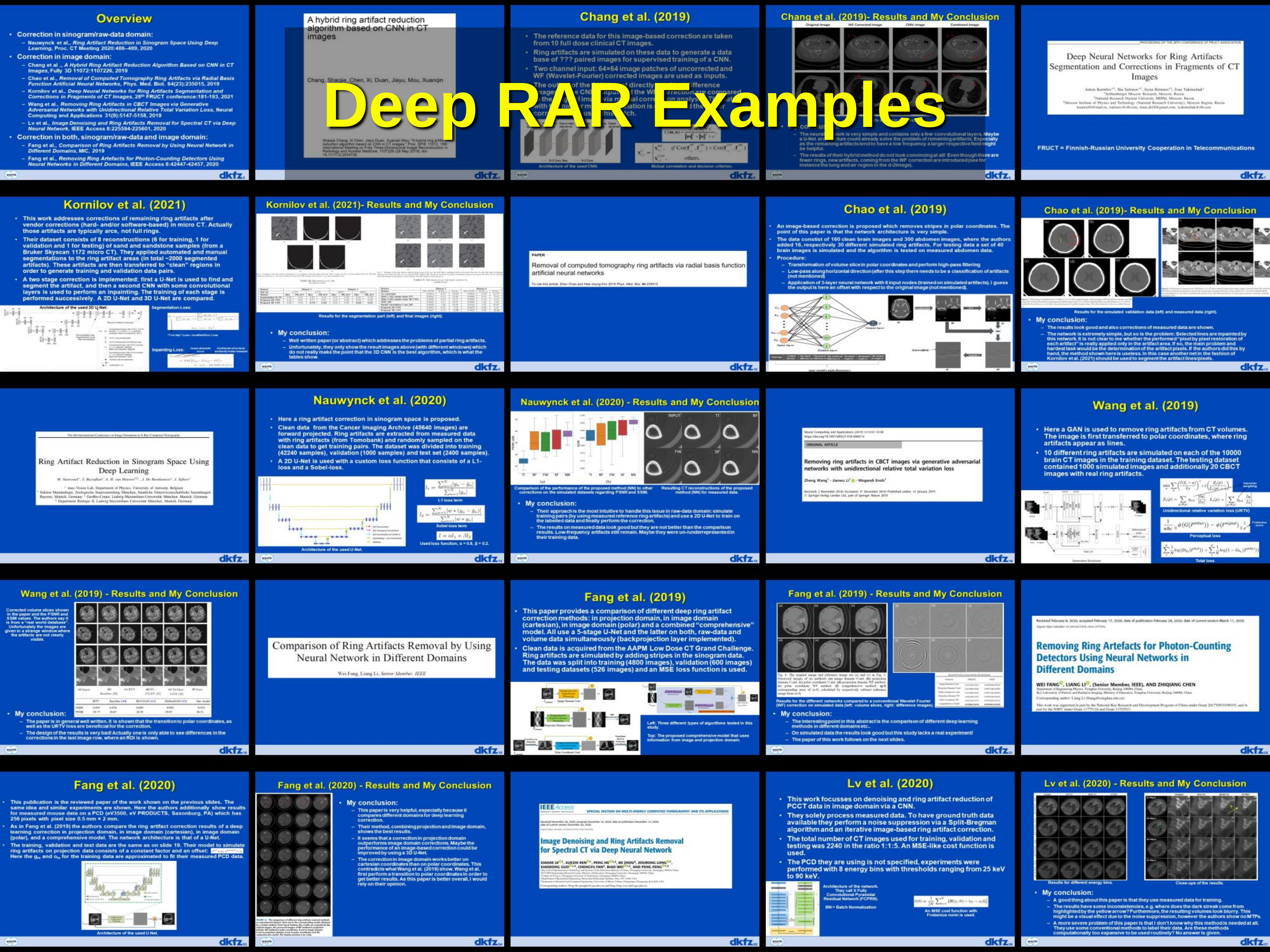
Deep RAR Examples
Overview
Chang et al. (2019)
Chang et al. (2019)- Results and My Conclusion
Kornilov et al. (2021)
Kornilov et al. (2021)- Results and My Conclusion
Chao et al. (2019)
Chao et al. (2019)- Results and My Conclusion
Nauwynck et al. (2020)
Nauwynck et al. (2020) - Results and My Conclusion
Wang et al. (2019)
Wang et al. (2019) - Results and My Conclusion
Fang et al. (2019)
Fang et al. (2019) - Results and My Conclusion
Fang et al. (2020)
Fang et al. (2020) - Results and My Conclusion
Lv et al. (2020)
Lv et al. (2020) - Results and My Conclusion

Ring Artifact Reduction: Literature

- **Correction in sinogram/rawdata domain:**
  - **Nauwynck et al., *Ring Artifact Reduction in Sinogram Space Using Deep Learning*, Proc. CT Meeting 2020:486–489, 2020**
- **Correction in image domain:**
  - **Chang et al ., *A Hybrid Ring Artifact Reduction Algorithm Based on CNN in CT Images*, Fully 3D 11072:1107226, 2019**
  - **Chao et al., *Removal of Computed Tomography Ring Artifacts via Radial Basis Function Artificial Neural Networks*, Phys. Med. Biol. 64(23):235015, 2019**
  - **Kornilov et al., *Deep Neural Networks for Ring Artifacts Segmentation and Corrections in Fragments of CT Images*, 28th FRUCT conference:181-193, 2021**
  - **Wang et al., *Removing Ring Artifacts in CBCT via GAN with Unidirectional Relative Total Variation Loss*, Neural Computing and Applications 31(9):5147-5158, 2019**
  - **Lv et al., *Image Denoising and Ring Artifacts Removal for Spectral CT via Deep Neural Network*, IEEE Access 8:225594-225601, 2020**
- **Correction in both, sinogram/raw-data and image domain:**
  - **Fang et al., *Comparison of Ring Artifacts Removal by Using Neural Network in Different Domains*, MIC, 2019**
  - **Fang et al., *Removing Ring Artefacts for Photon-Counting Detectors Using Neural Networks in Different Domains*, IEEE Access 8:42447-42457, 2020**

Ring Artifact Reduction: Comments

- **Correction in sinogram/rawdata domain:**
  - **Nauwynck et al. (2020) – Results are ok. The method can, however, not correct low-frequency ring artifacts.**
- **Correction in image domain:**
  - **Chang et al. (2019) – Strange mixture of CNN and classical method. New artifacts are introduced.**
  - **Chao et al. (2019) – It remains unclear how the artifact areas are segmented. Only zoom-ins show some improvements.**
  - **Kornilov et al. (2021) – Theoretically sound, however, no reasonable images are presented.**
  - **Wang et al. (2019) – The results of all correction methods look the same (suboptimal gray scale windowing).**
  - **Lv et al. (2020) – The question arises why the method to generate the ground-truth data is not directly used for correction.**
- **Correction in both, sinogram/raw-data and image domain:**
  - **Fang et al. (2019) – The results shown are interesting. However, there are no measured data processed.**
  - **Fang et al. (2020) – The results are good. Probably it is the best method of this slide's list.**

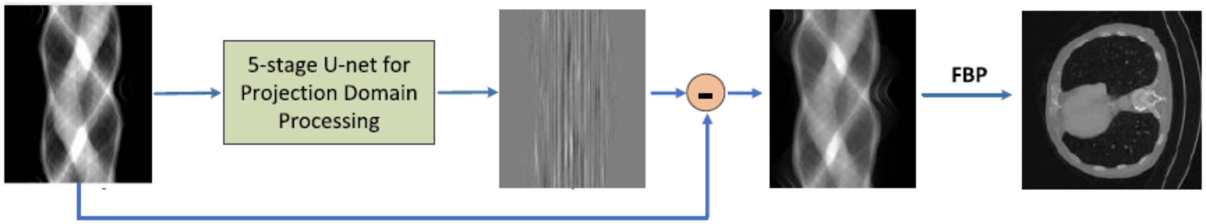

FIGURE 3. The diagram of ring artefacts removal in projection domain.

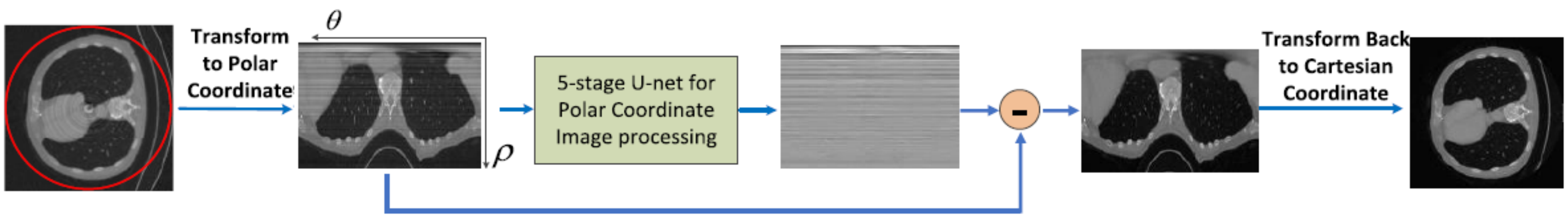

FIGURE 4. The diagram of ring artefacts removal in polar coordinate system.

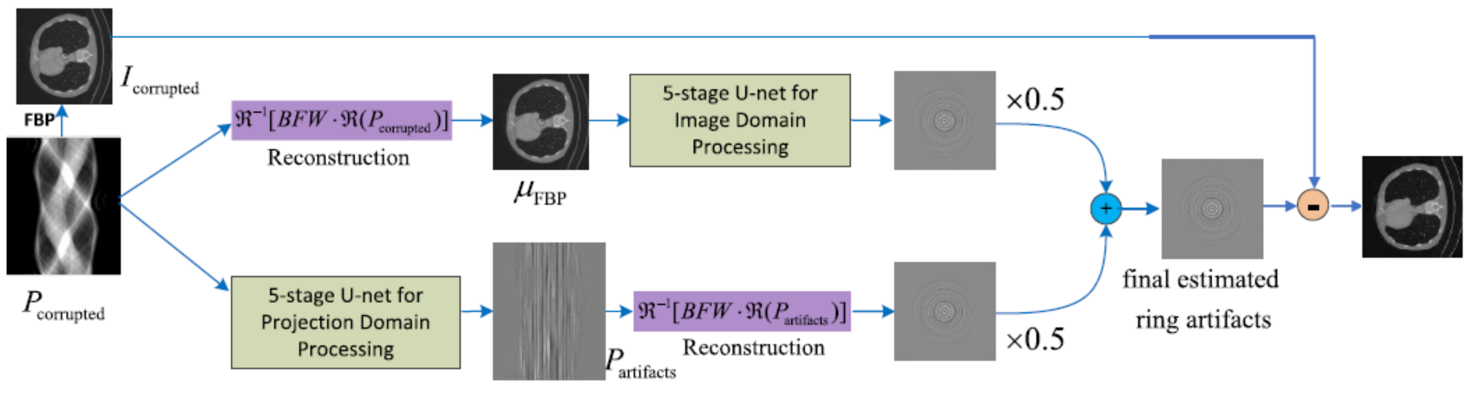

FIGURE 5. The diagram of ring artefacts removal using a comprehensive model.

Fang, Li, and Chen. Removing Ring Artefacts for Photon-Counting Detectors Using Neural Networks in Different Domains. IEEE Access 8:42447-42457, 2020.

Wavelet projection domain

Wavelet polar image domain

U-net image domain

U-net projection domain

U-net polar image domain

U-net in both domains

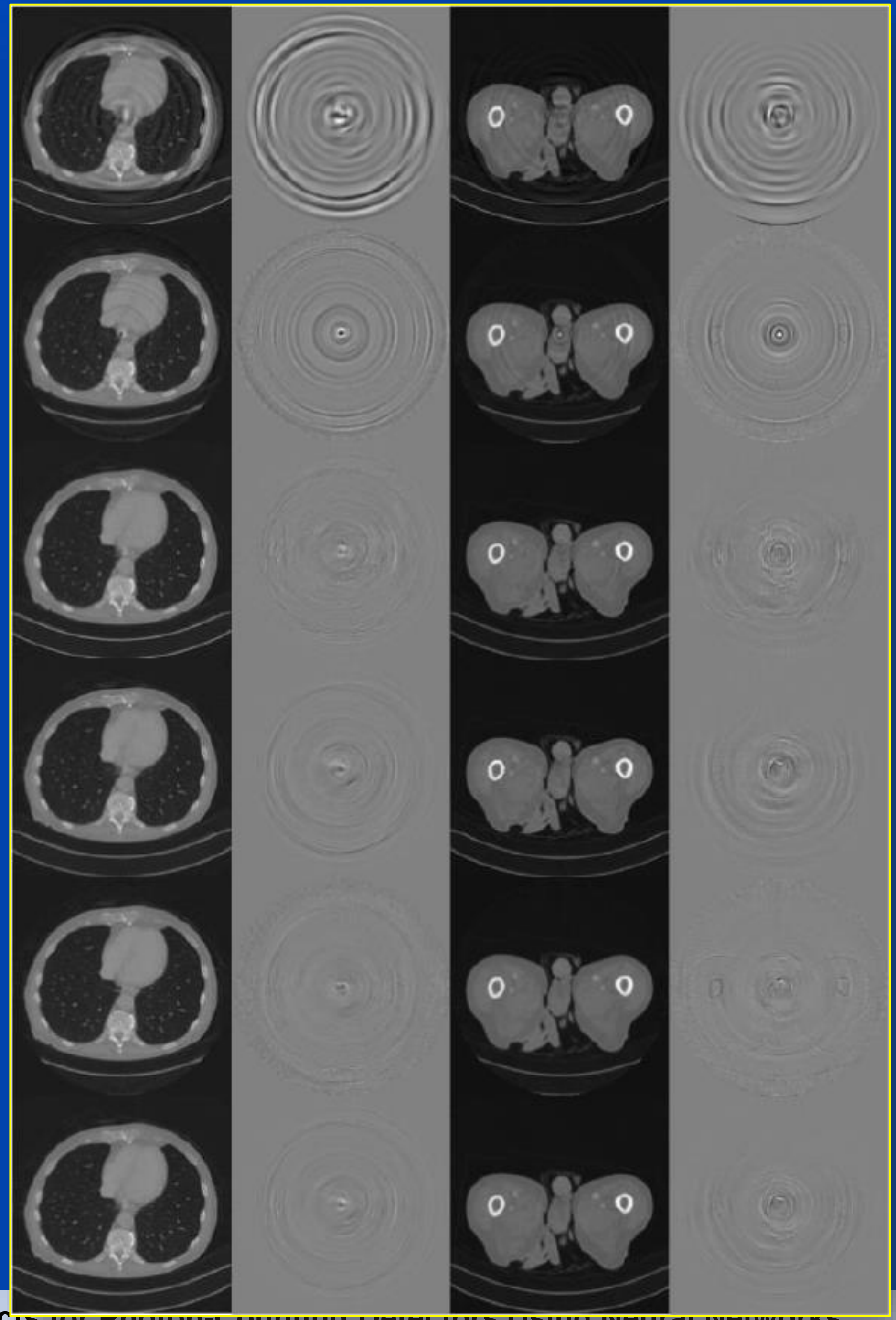

Fang, Li, and Chen. Removing Ring Artefacts for Photon-Counting Detectors Using Neural Networks in Different Domains. IEEE Access 8:42447-42457, 2020.

Summary on Deep RAR

- Similar comments as for deep MAR apply here.
- Often, the images are resampled to polar coordinates before being manipulated by the network.
- Deep learning, as of today, provides incremental improvements compared to conventional RAR methods.

Deep Detruncation

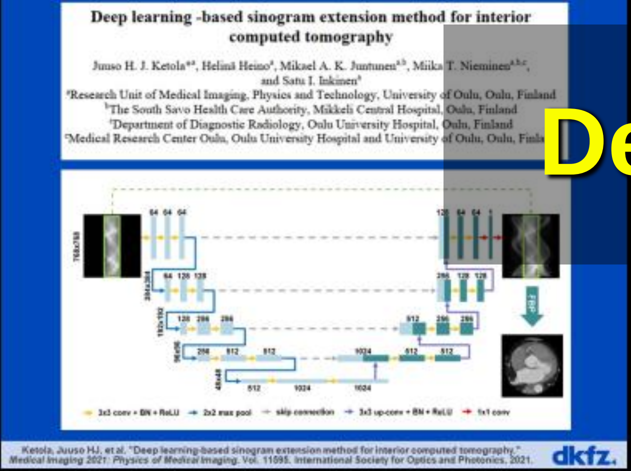

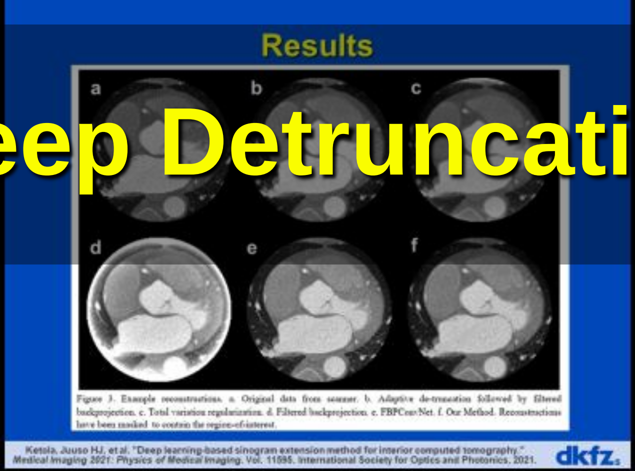

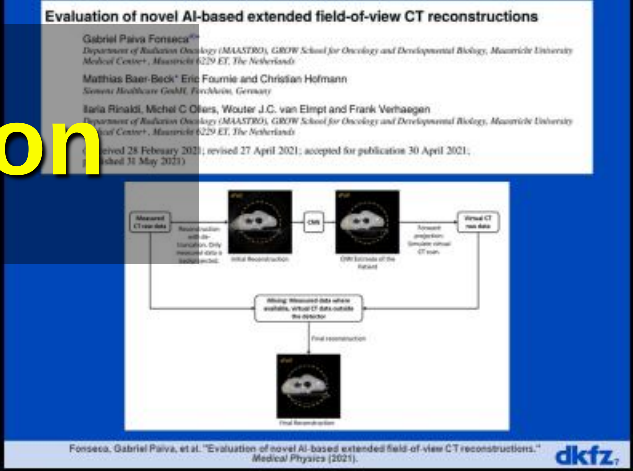

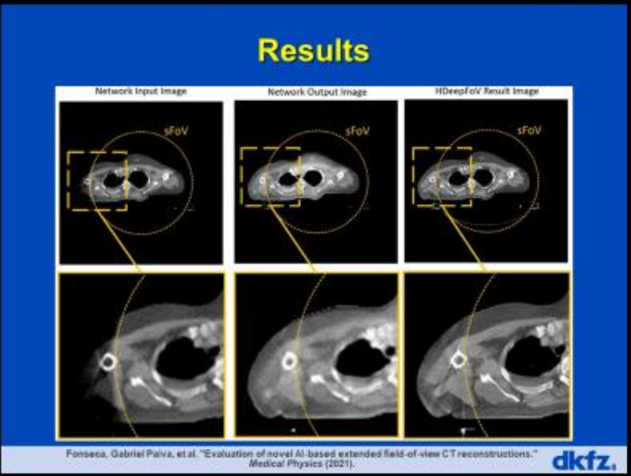

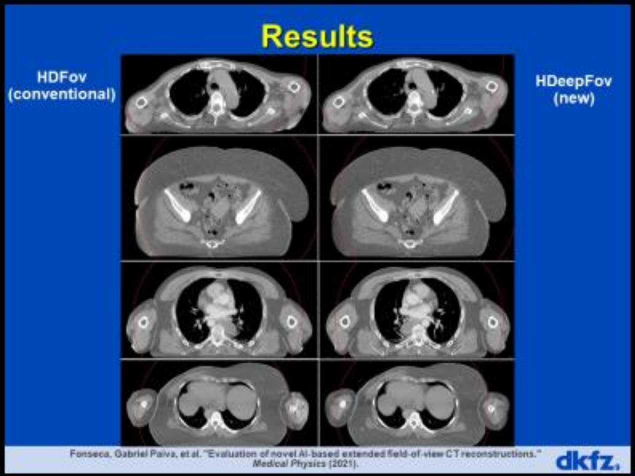

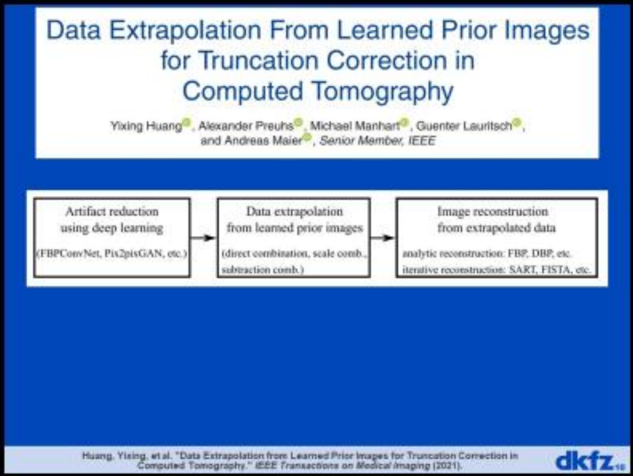

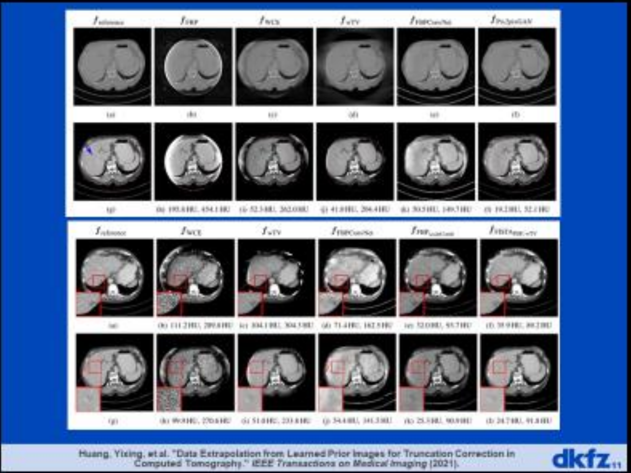

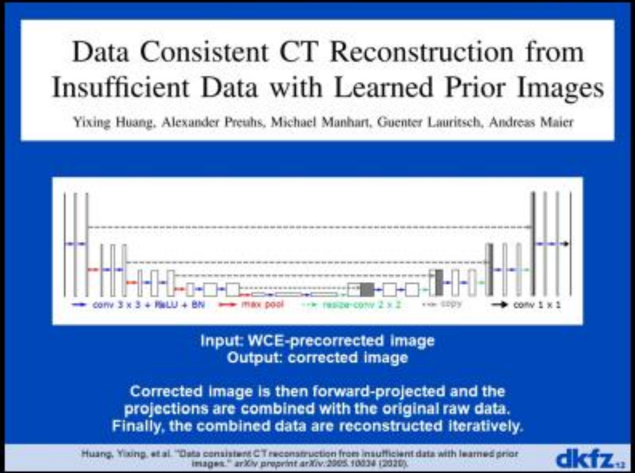

Deep learning -based sinogram extension method for interior computed tomography

Juuso H. J. Ketola*[a], Helinä Heino[a], Mikael A. K. Juntunen[a,b], Miika T. Nieminen[a,b,c], and Satu I. Inkinen[a]
[a]Research Unit of Medical Imaging, Physics and Technology, University of Oulu, Oulu, Finland
[b]The South Savo Health Care Authority, Mikkeli Central Hospital, Oulu, Finland
[c]Department of Diagnostic Radiology, Oulu University Hospital, Oulu, Finland
[c]Medical Research Center Oulu, Oulu University Hospital and University of Oulu, Oulu, Finland

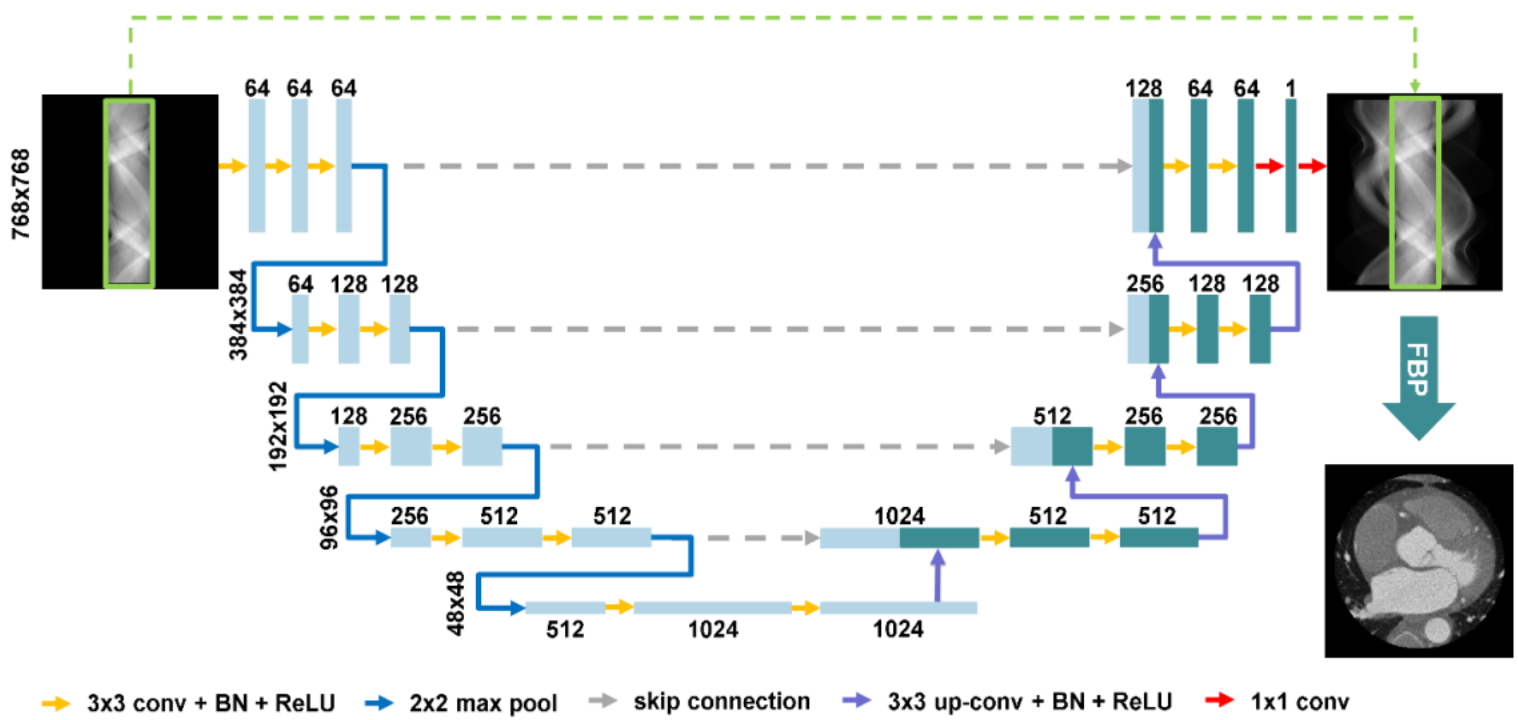

Ketola, Juuso HJ, et al. "Deep learning-based sinogram extension method for interior computed tomography." *Medical Imaging 2021: Physics of Medical Imaging*. Vol. 11595. International Society for Optics and Photonics, 2021.

dkfz.

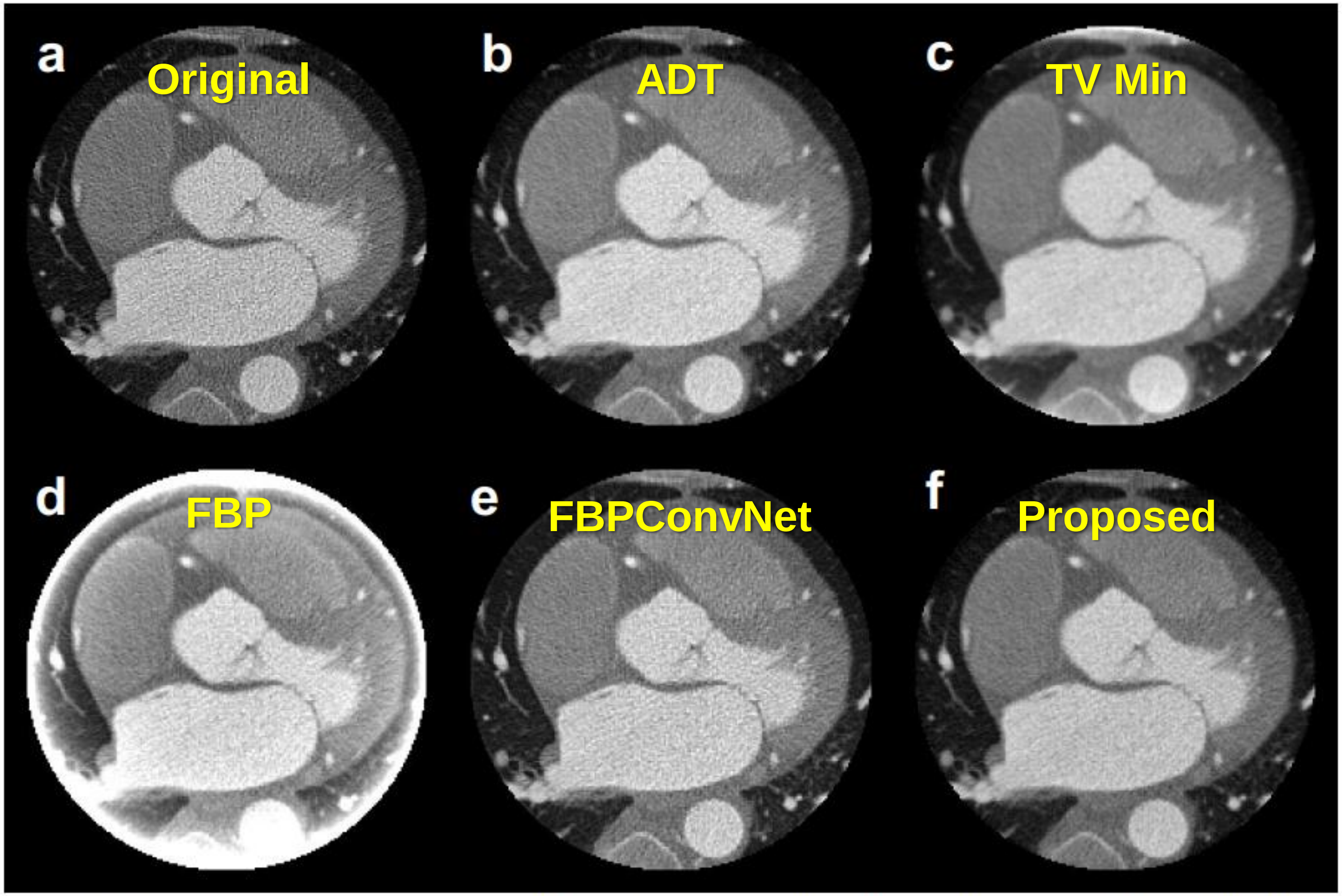

Figure 3. Example reconstructions. a. Original data from scanner. b. Adaptive de-truncation followed by filtered backprojection. c. Total variation regularization. d. Filtered backprojection. e. FBPConvNet. f. Our Method. Reconstructions have been masked to contain the region-of-interest.

Ketola, Juuso HJ, et al. "Deep learning-based sinogram extension method for interior computed tomography."
***Medical Imaging 2021: Physics of Medical Imaging*. Vol. 11595. International Society for Optics and Photonics, 2021.**

Evaluation of novel AI-based extended field-of-view CT reconstructions

Gabriel Paiva Fonseca[a)*]
Department of Radiation Oncology (MAASTRO), GROW School for Oncology and Developmental Biology, Maastricht University Medical Centre+, Maastricht 6229 ET, The Netherlands

Matthias Baer-Beck[*] Eric Fournie and Christian Hofmann
Siemens Healthcare GmbH, Forchheim, Germany

Ilaria Rinaldi, Michel C Ollers, Wouter J.C. van Elmpt and Frank Verhaegen
Department of Radiation Oncology (MAASTRO), GROW School for Oncology and Developmental Biology, Maastricht University Medical Centre+, Maastricht 6229 ET, The Netherlands

(Received 28 February 2021; revised 27 April 2021; accepted for publication 30 April 2021; published 31 May 2021)

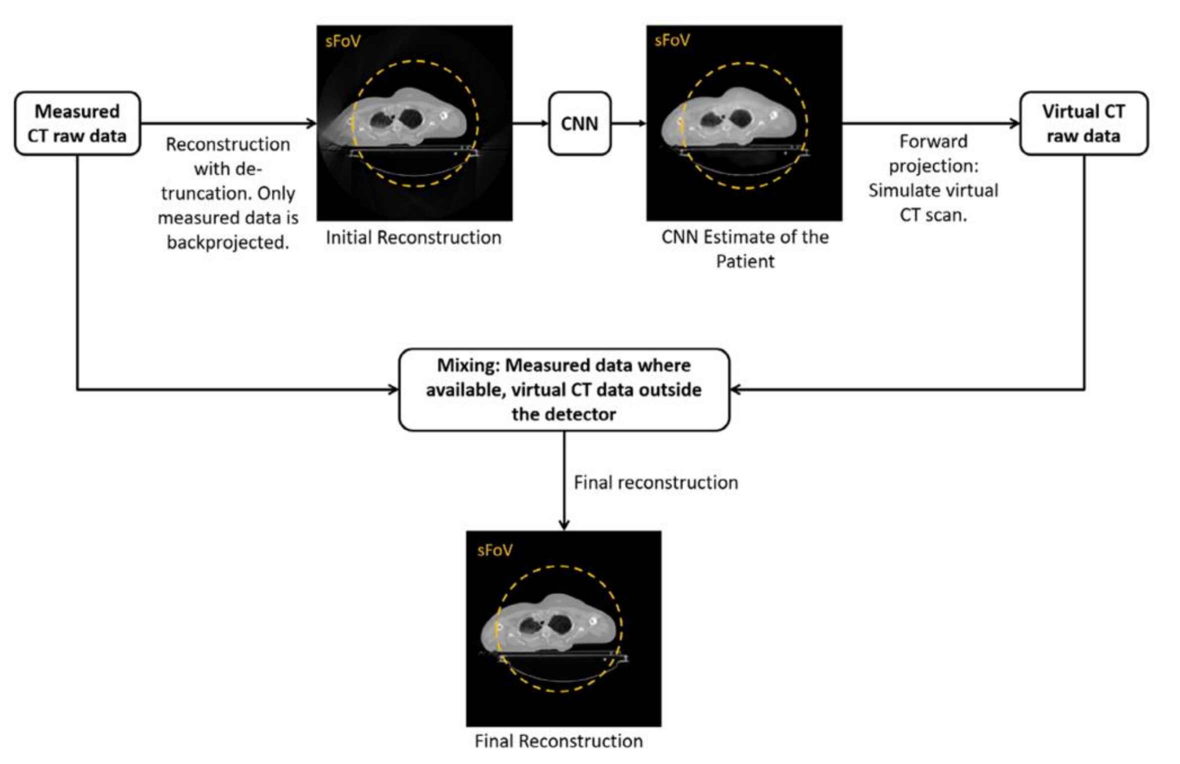

Fonseca, Gabriel Paiva, et al. "Evaluation of novel AI-based extended field-of-view CT reconstructions." *Medical Physics* (2021).

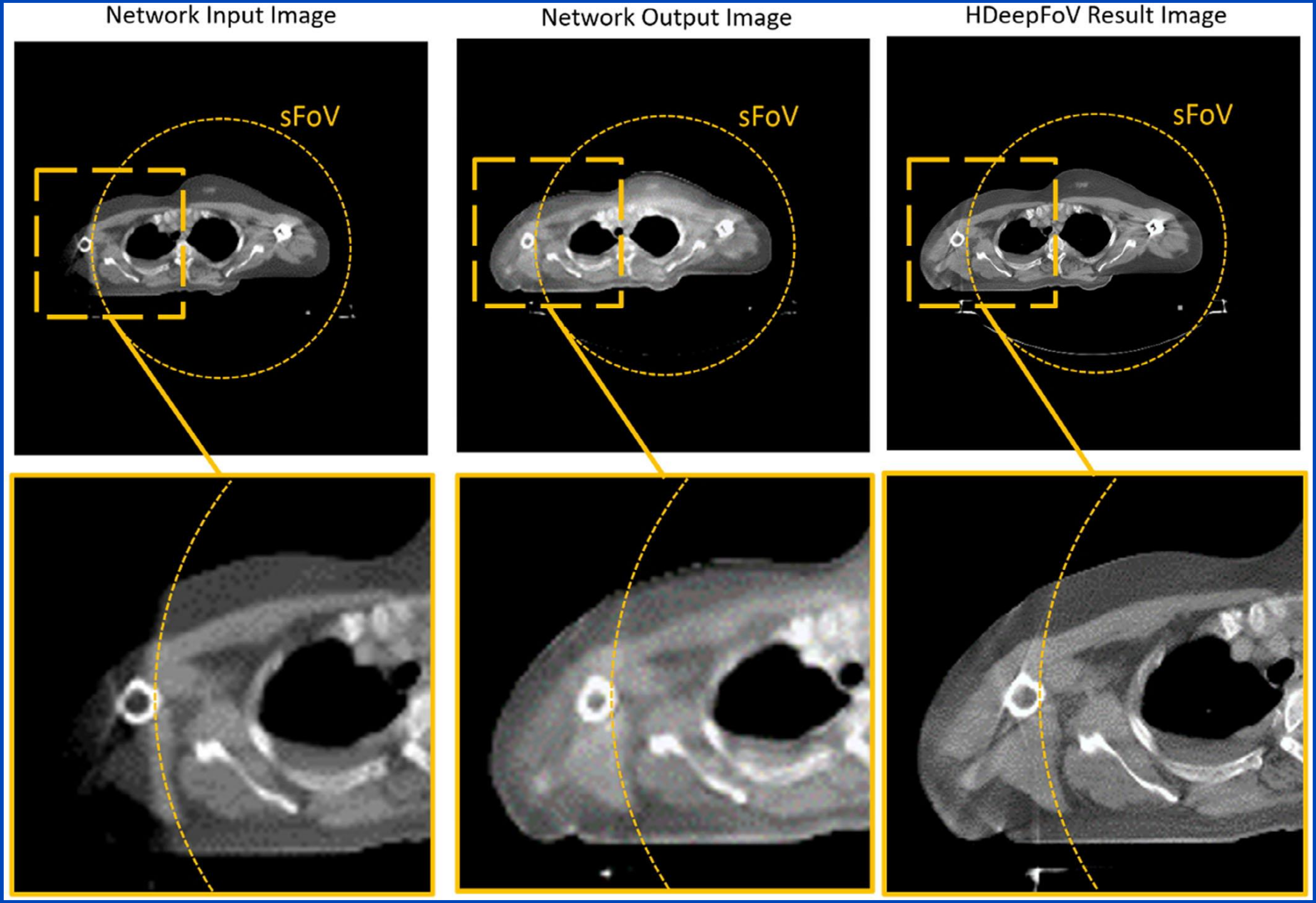

Fonseca, Gabriel Paiva, et al. "Evaluation of novel AI-based extended field-of-view CT reconstructions."
Medical Physics (2021).

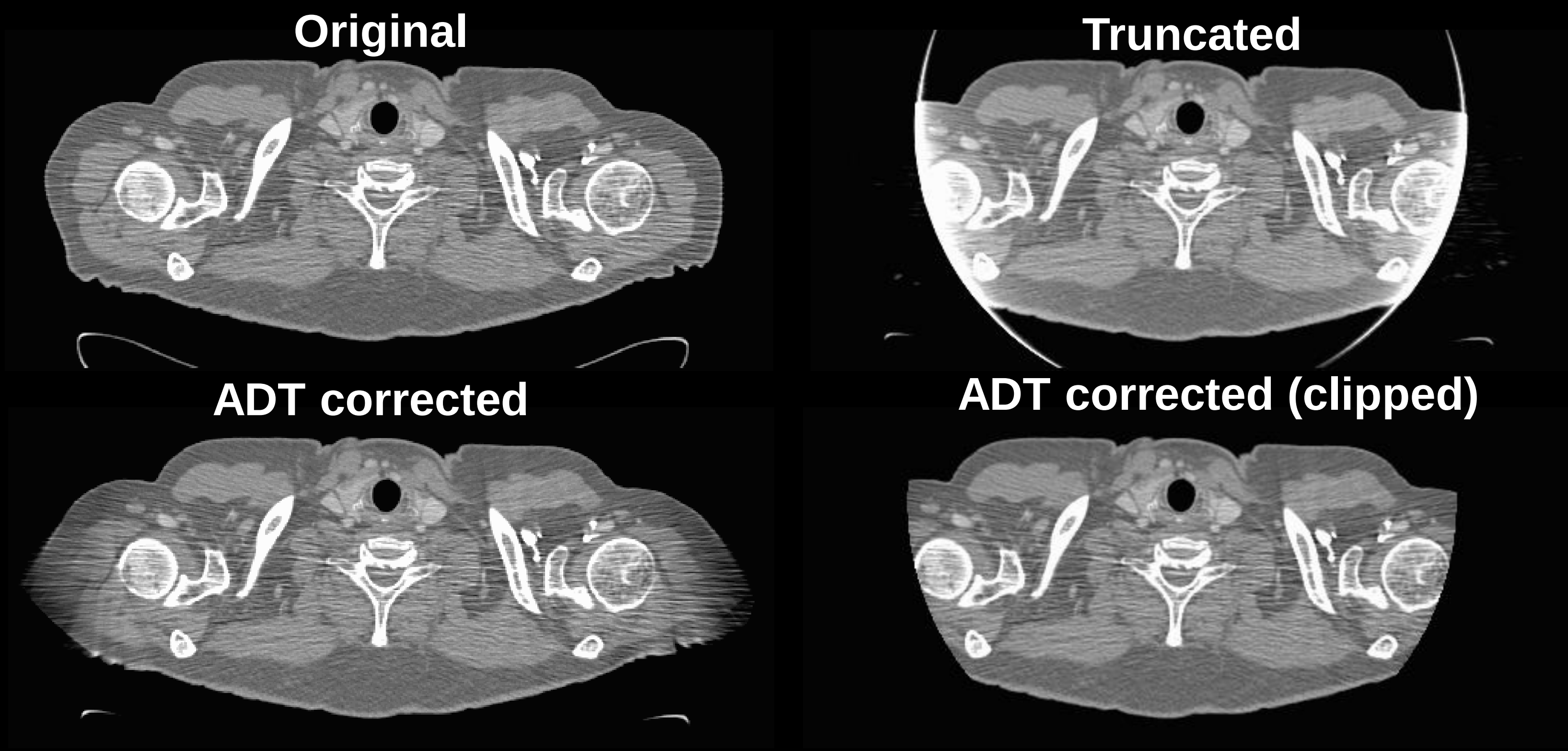

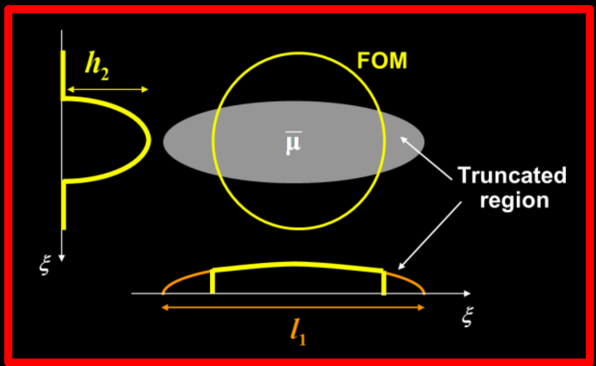

C = 0 HU, W = 1000 HU

K. Sourbelle, M. Kachelrieß, and W.A. Kalender, "Reconstruction from truncated projections in CT using adaptive detruncation," Eur Radiol 15:1008–1014, 2005.

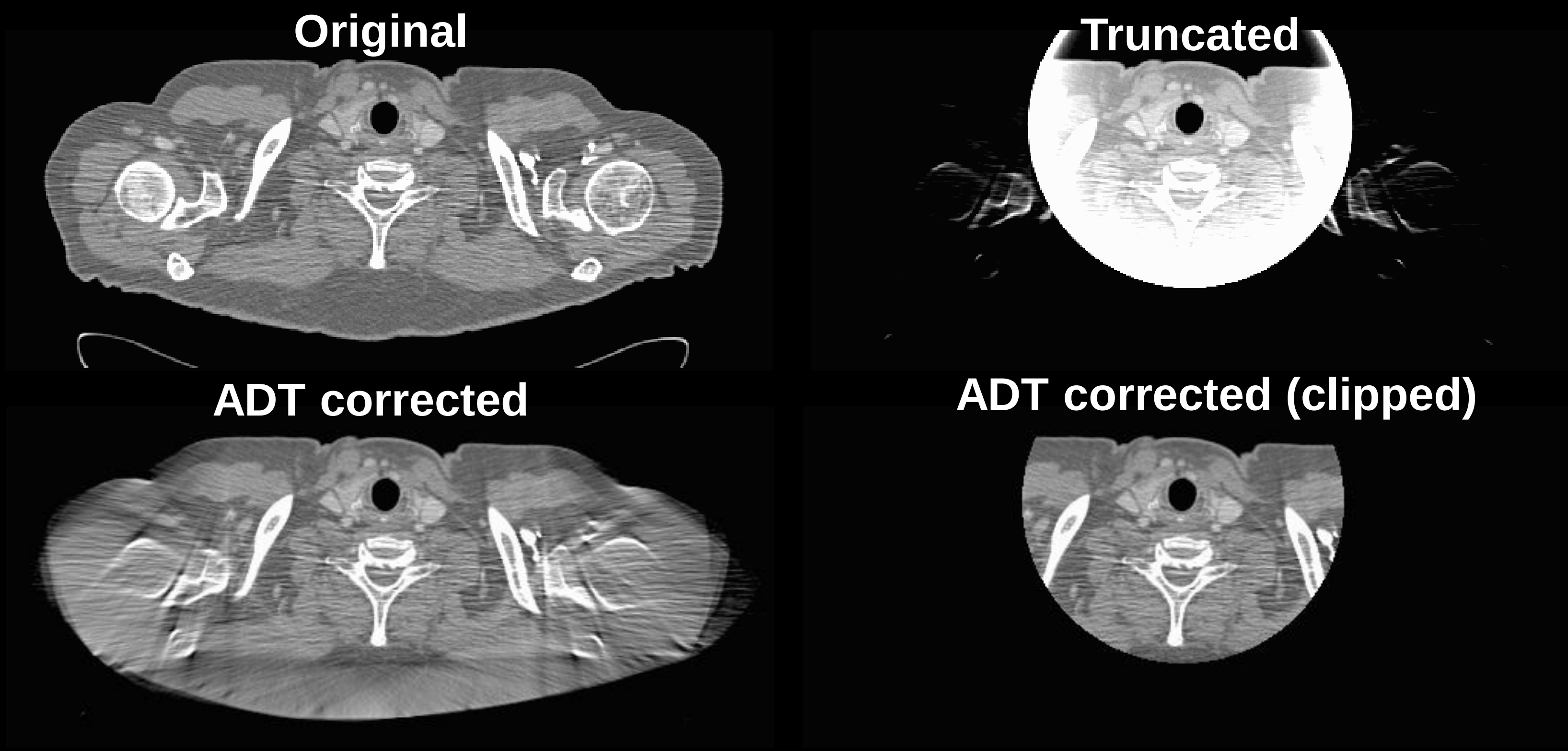

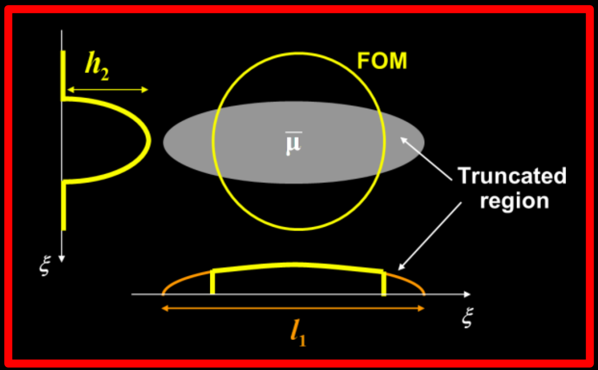

C = 0 HU, W = 1000 HU

K. Sourbelle, M. Kachelrieß, and W.A. Kalender, "Reconstruction from truncated projections in CT using adaptive detruncation," Eur Radiol 15:1008–1014, 2005.

Summary on Deep Detruncation

- No need for machine learning to restore the gray values within the FOM
- Image domain cosmetic detruncation can serve as an intermediate step to detruncate CT data.

Deep Scatter Estimation

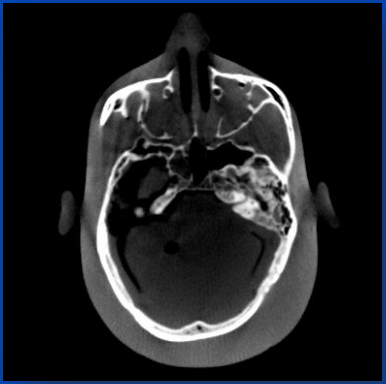

???

In real time?

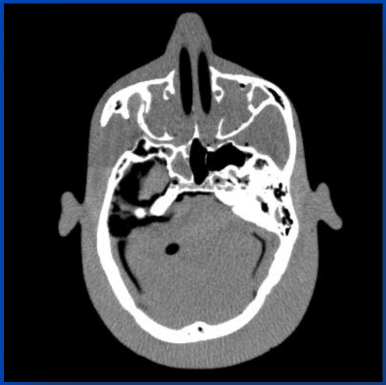

Monte Carlo Scatter Estimation

- Simulation of photon trajectories according to physical interaction probabilities.
- Simulating a large numb ories well approximat

1 hour
per tomographic data set

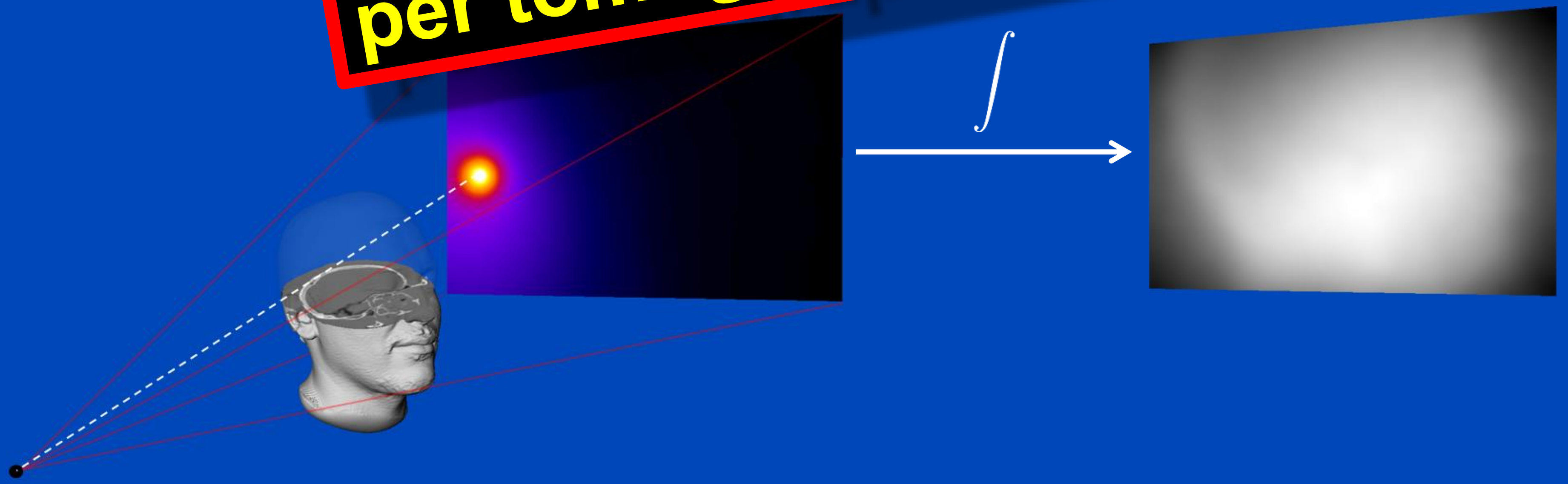

Deep Scatter Estimation

Network architecture & scatter estimation framework

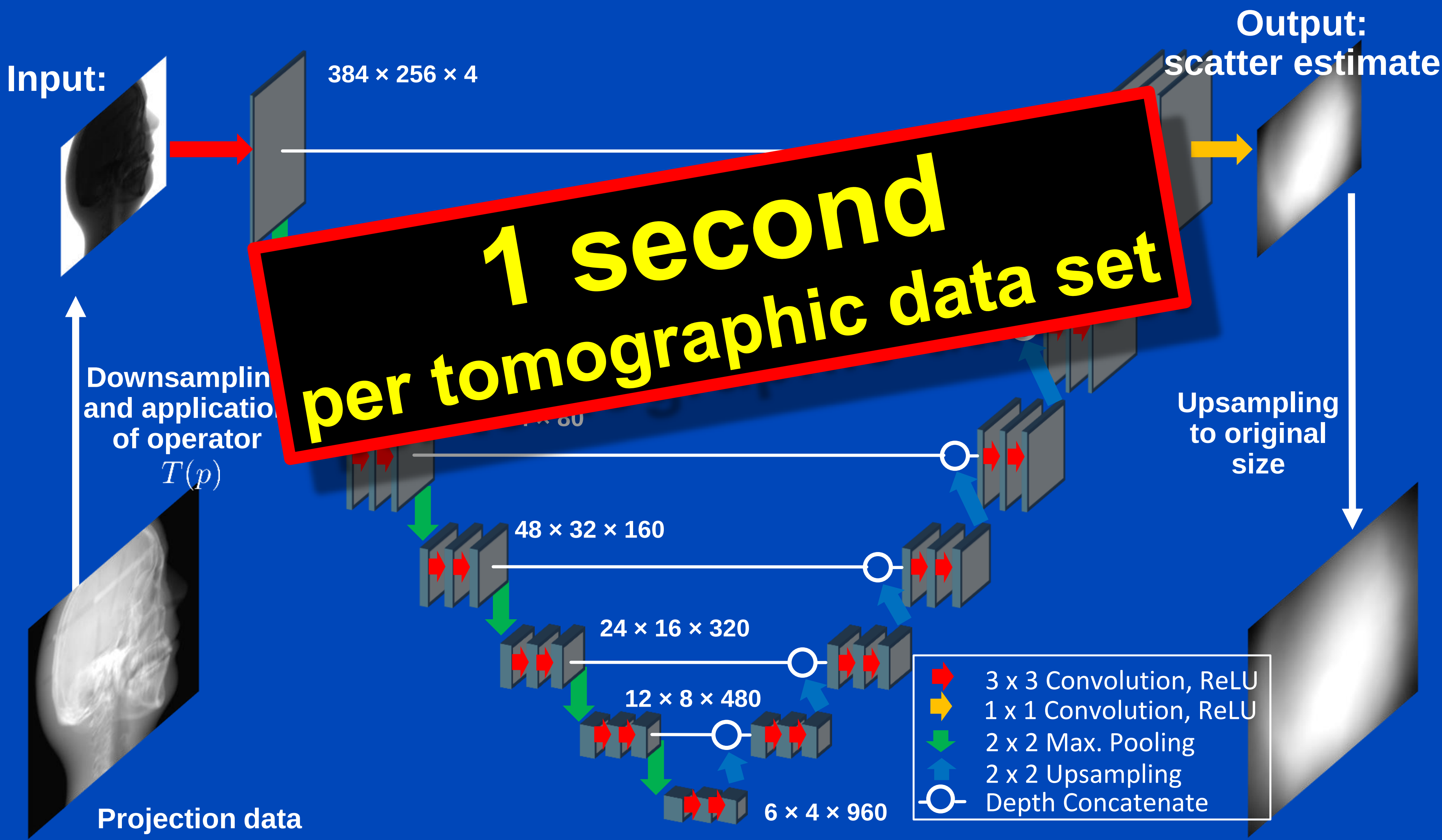

1 second
per tomographic data set

J. Maier, M. Kachelrieß et al. Deep scatter estimation (DSE). SPIE 2017 and Journal of Nondestructive Evaluation 37:57, July 2018.
J. Maier, M. Kachelrieß et al. Robustness of DSE. Med. Phys. 46(1):238-249, January 2019.

Testing of the DSE Network for Measured Data (120 kV)

DKFZ table-top CT

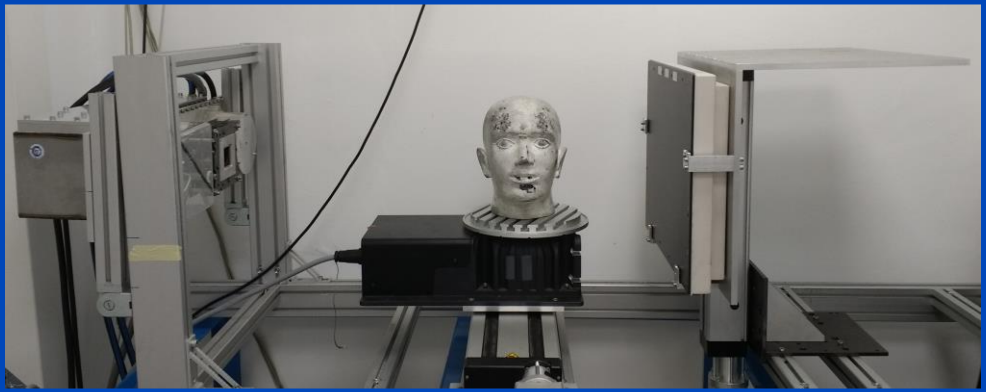

- Measurement of a head phantom at our in-house table-top CT.
- Slit scan measurement serves as ground truth.

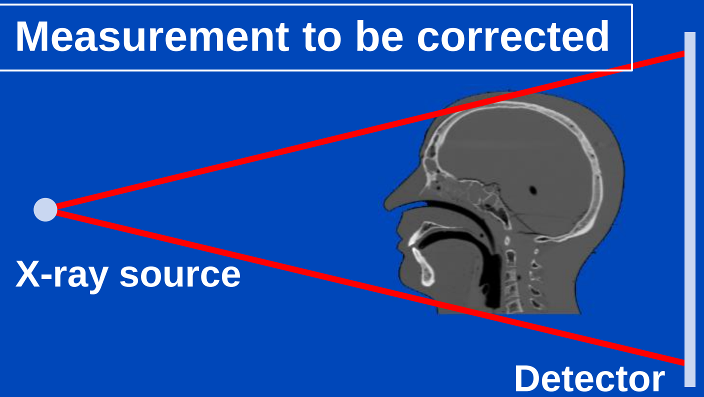

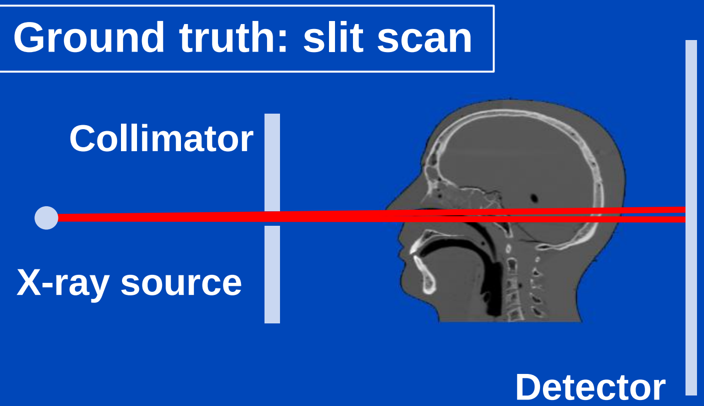

J. Maier, M. Kachelrieß et al. Deep scatter estimation (DSE). SPIE 2017 and Journal of Nondestructive Evaluation 37:57, July 2018.
J. Maier, M. Kachelrieß et al. Robustness of DSE. Med. Phys. 46(1):238-249, January 2019.

Reconstructions of Measured Data

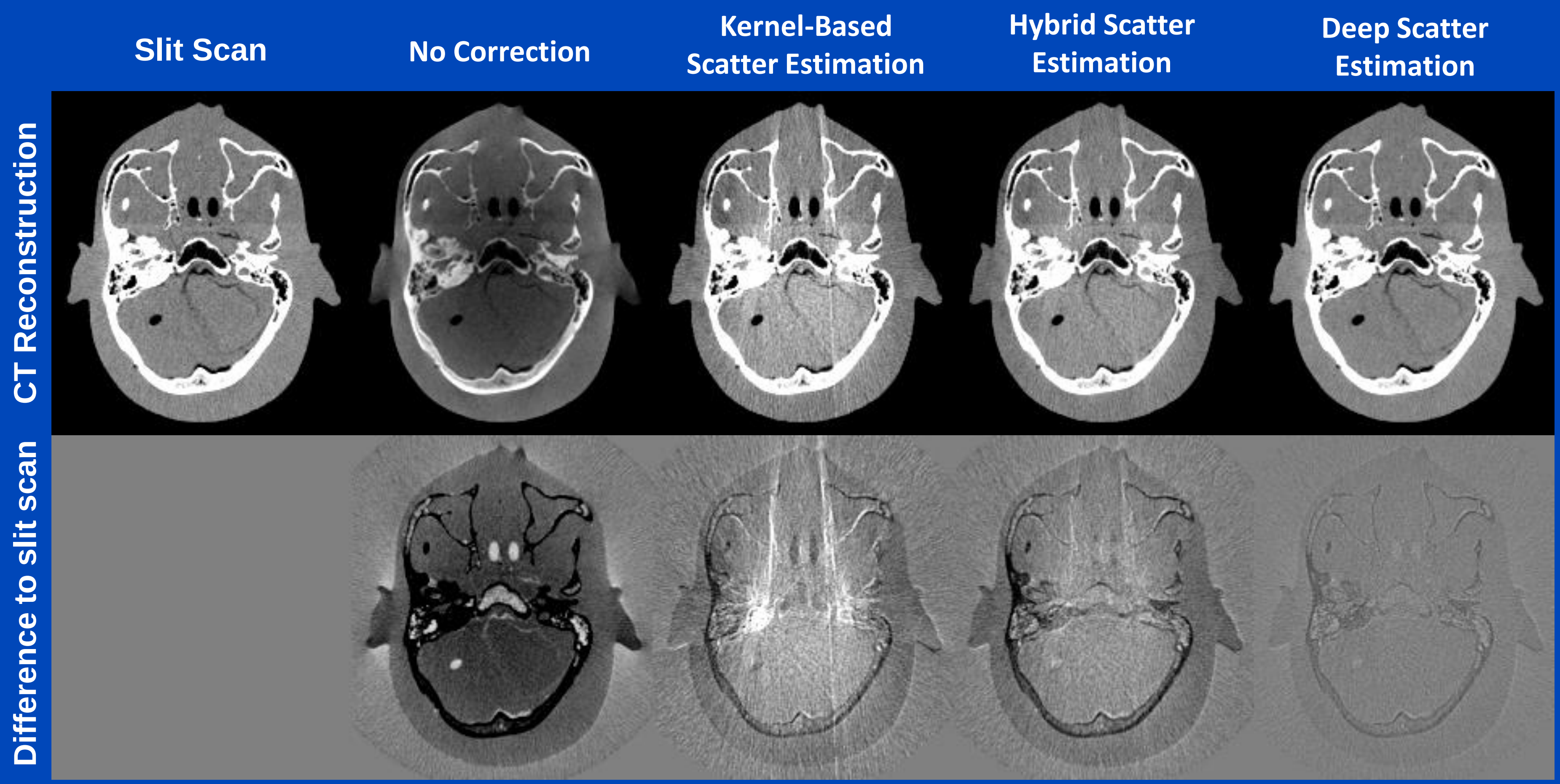

C = 0 HU, W = 1000 HU

A simple detruncation was applied to the rawdata before reconstruction. Images were clipped to the FOM before display. *C* = -200 HU, *W* = 1000 HU.

Truncated DSE

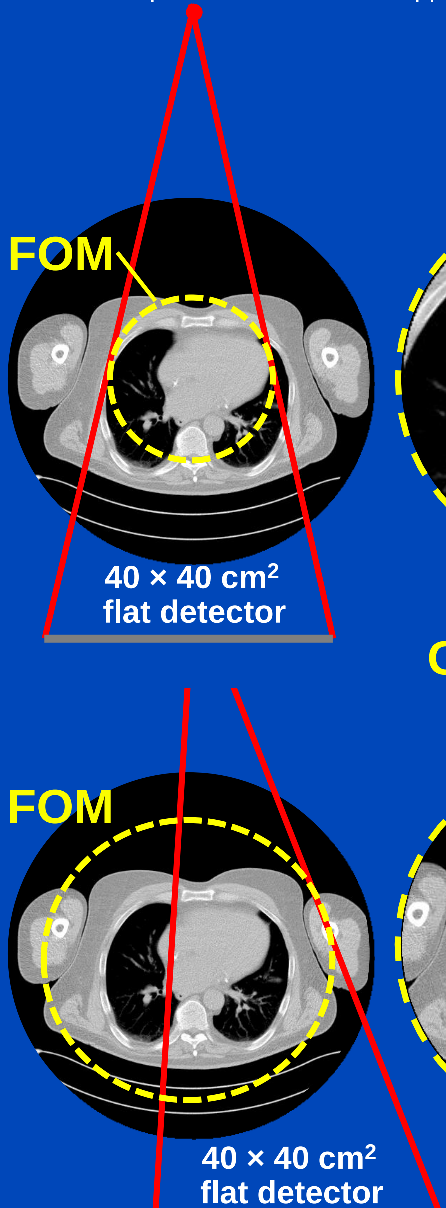

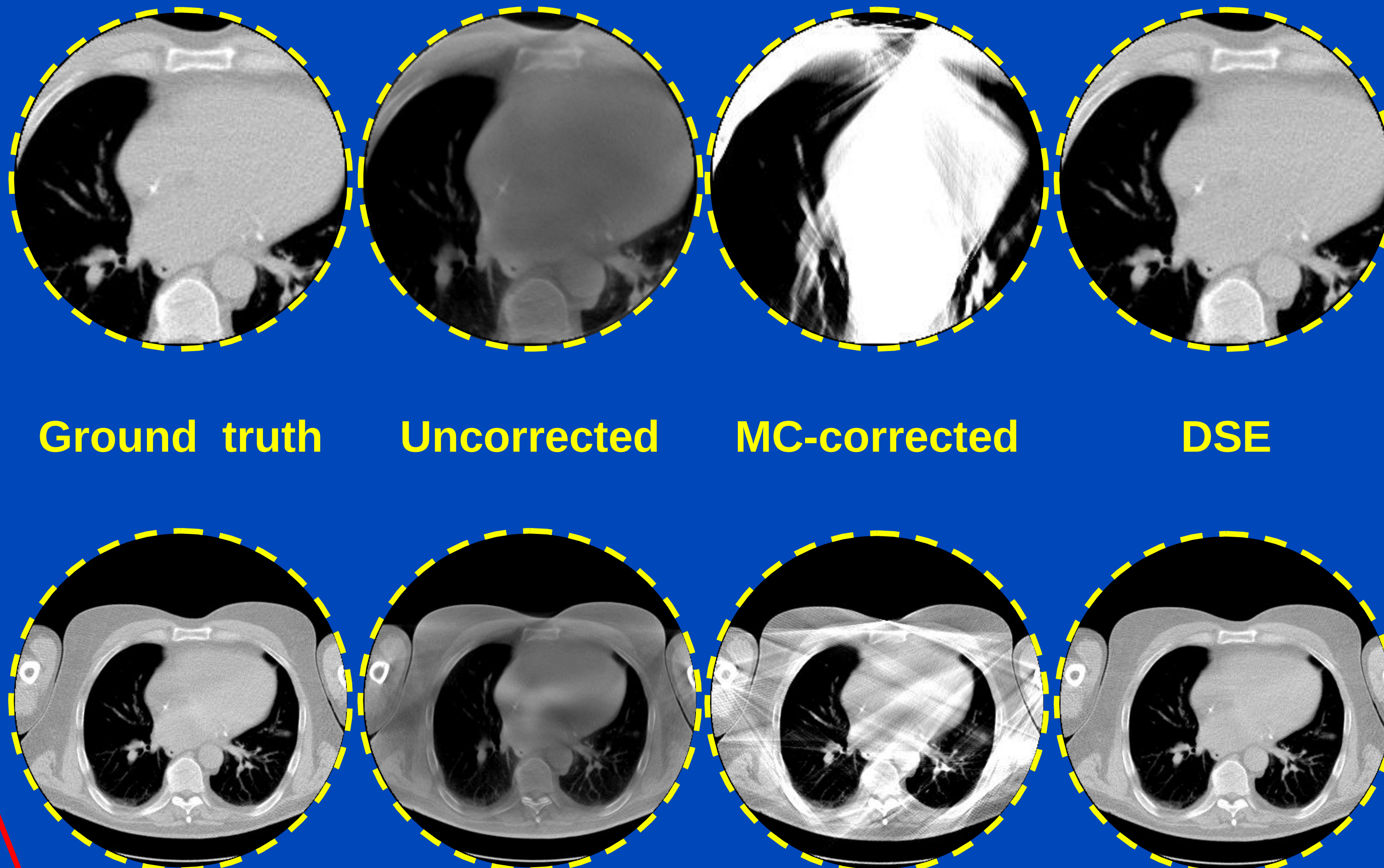

To learn why MC fails at truncated data and what significant efforts are necessary to cope with that situation see [Kachelrieß et al. Effect of detruncation on the accuracy of MC-based scatter estimation in truncated CBCT. Med. Phys. 45(8):3574-3590, August 2018].

J. Maier, M. Kachelrieß et al. Deep scatter estimation (DSE). SPIE 2017 and Journal of Nondestructive Evaluation 37:57, July 2018.
J. Maier, M. Kachelrieß et al. Robustness of DSE. Med. Phys. 46(1):238-249, January 2019.

Results

	Testing Head	Thorax	Abdomen
Training			
KSE			
Head	14.5	26.8	32.5
Thorax	16.2	18.5	19.4
Abdomen	16.8	22.1	17.8
All data	14.9	20.5	19.3
HSE (Truncated prior, 22 cm FOM)			
-	6.2	293.2	237.6
HSE (Truncated prior, shifted detector, 40 cm FOM)			
-	-	22.9	26.5
DSE, $M_{\mathrm{ep}} : e^{-p_{\mathrm{sim}}} \longrightarrow S_{\mathrm{MC}}$			
Head	3.9	17.6	23.5
Thorax	12.2	2.5	11.6
Abdomen	27.1	13.2	2.3
All data	4.7	2.5	2.4
DSE, $M_{\mathrm{p}} : p_{\mathrm{sim}} \longrightarrow S_{\mathrm{MC}}$			
Head	1.3	14.9	15.2
Thorax	6.7	1.6	7.7
Abdomen	15.7	12.1	1.5
All data	1.7	1.6	1.6
DSE, $M_{\mathrm{pep}} : p_{\mathrm{sim}} \cdot e^{-p_{\mathrm{sim}}} \longrightarrow S_{\mathrm{MC}}$			
Head	1.2	21.1	32.7
Thorax	8.8	1.5	9.1
Abdomen	11.9	10.9	1.3
All data	1.8	1.4	1.4

Mean absolute percentage error of the kernel-based scatter estimation (KSE), the hybrid scatter estimation (HSE) and the deep scatter estimation (DSE) with respect to the ground truth scatter distribution (MC simulation). Training data were generated simulating head, thorax and abdomen data at 120 kV, 140 kV. The training was performed for head, thorax and abdomen data separately as well as using all data together (left column). DSE was trained for three different mappings ($M_{\mathrm{ep}} : e^{-p_{\mathrm{sim}}} \rightarrow S_{\mathrm{MC}}$, $M_{\mathrm{p}} : p_{\mathrm{sim}} \rightarrow S_{\mathrm{MC}}$, $M_{\mathrm{pep}} : p \cdot e^{-p_{\mathrm{sim}}} \rightarrow S_{\mathrm{MC}}$). Note that there are no training data for the HSE as it is optimized on a coarse MC simulation of the testing data.

Values shown are the mean absolute percentage errors (MAPEs) of the testing data.
Note that thorax and head suffer from truncation due to the small size of the 40×30 cm flat detector.

dkfz.

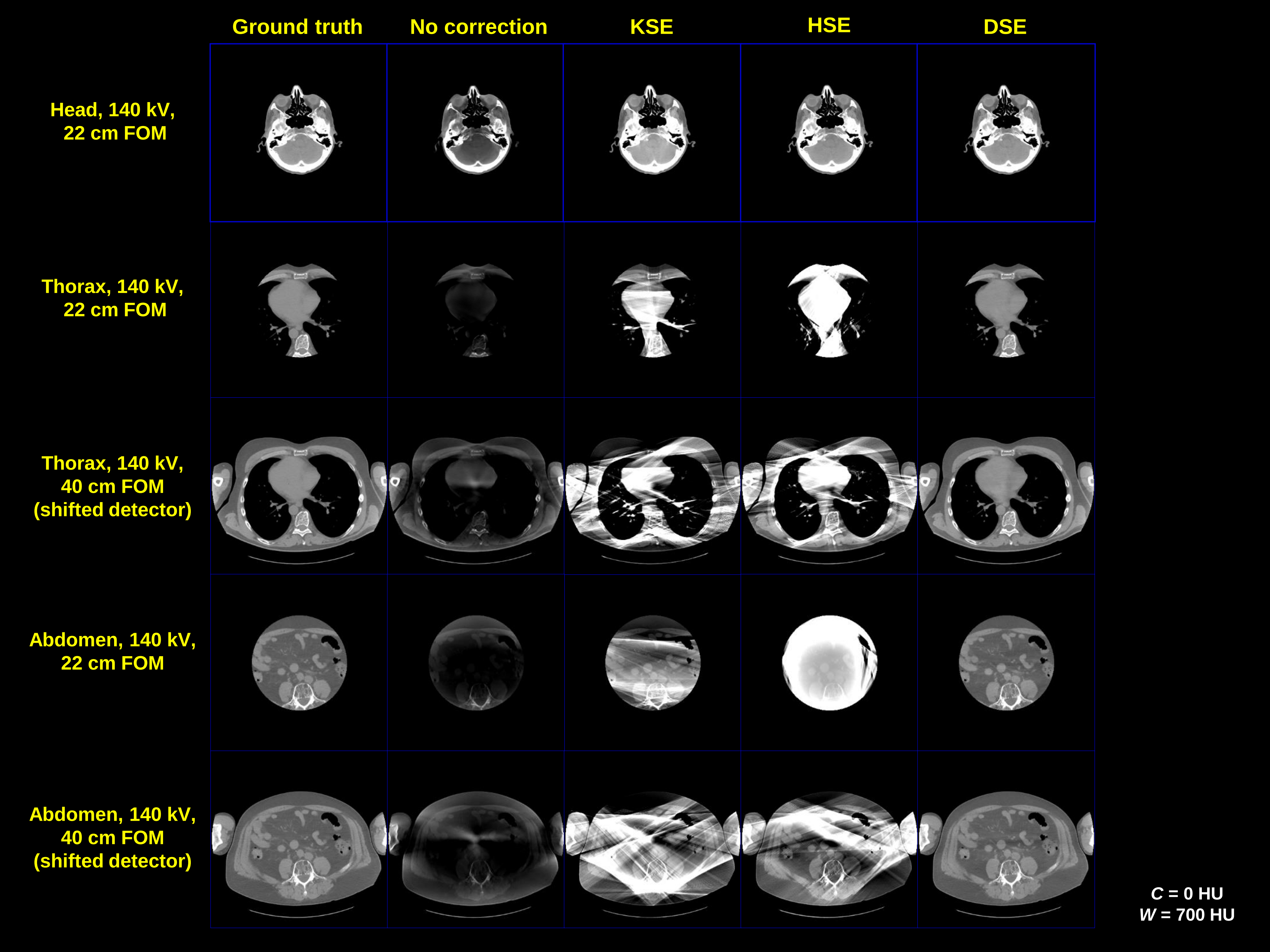

Ground truth
No correction
KSE
HSE
DSE
Head, 140 kV,
22 cm FOM
Thorax, 140 kV,
22 cm FOM
Thorax, 140 kV,
40 cm FOM
(shifted detector)
Abdomen, 140 kV,
22 cm FOM
Abdomen, 140 kV,
40 cm FOM
(shifted detector)
C = 0 HU
W = 700 HU

Scatter in Dual Source CT (DSCT)

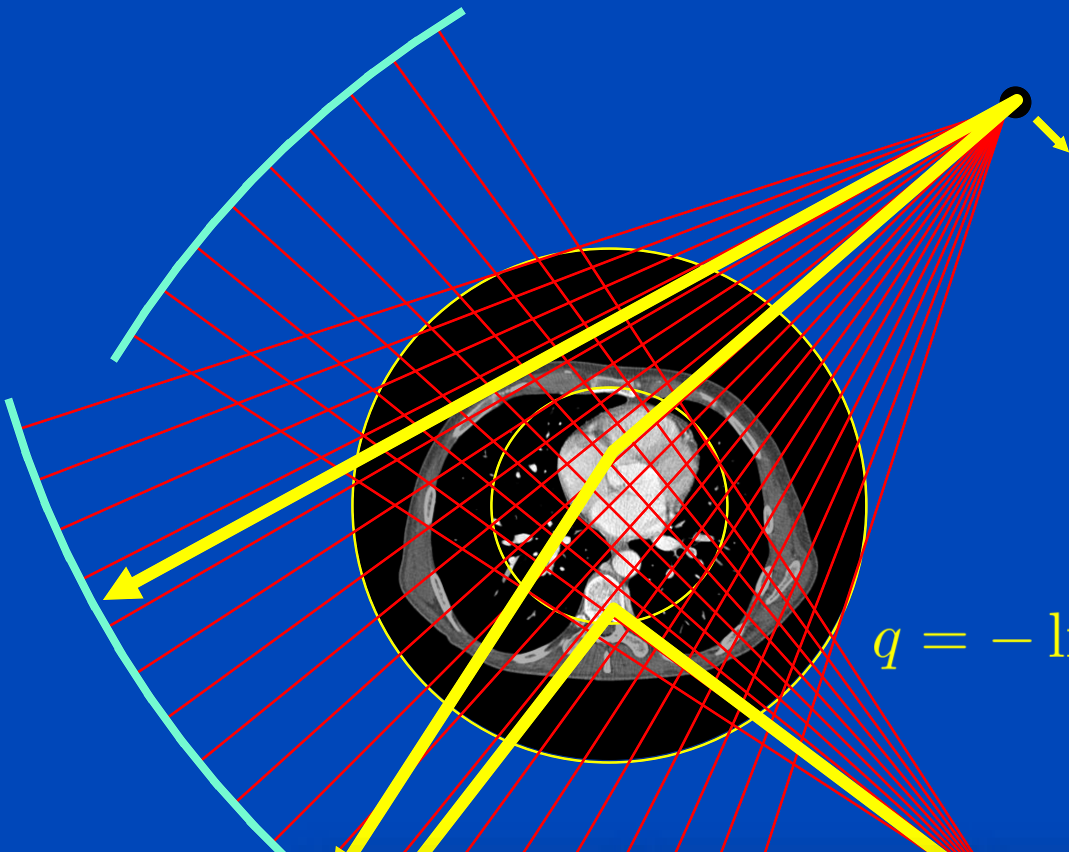

Siemens SOMATOM Force
dual source cone-beam spiral CT

$$q = -\ln \frac{I_{\text{primary}} + S_{\text{forward}} + \rho\, S_{\text{cross}}}{I_0}$$

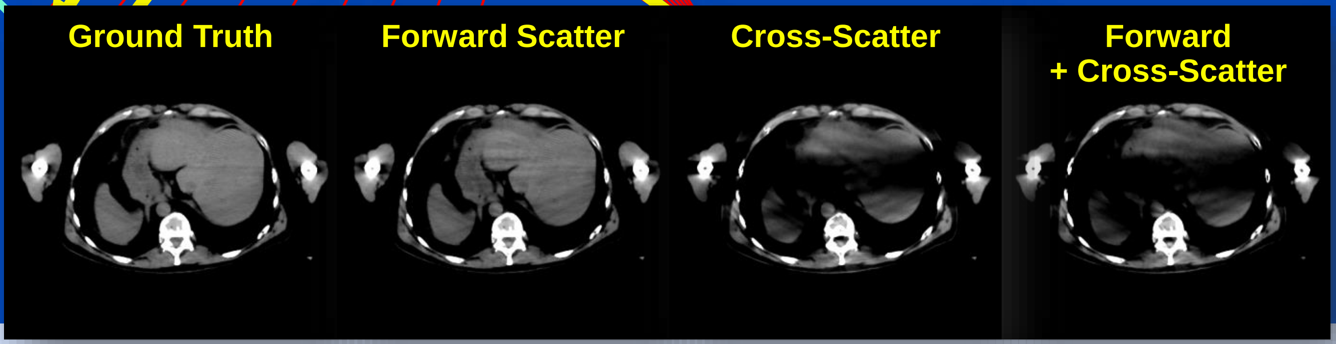

C = 40 HU, *W* = 300 HU, with 2D anti-scatter grid

Scatter in Dual Source CT (DSCT)

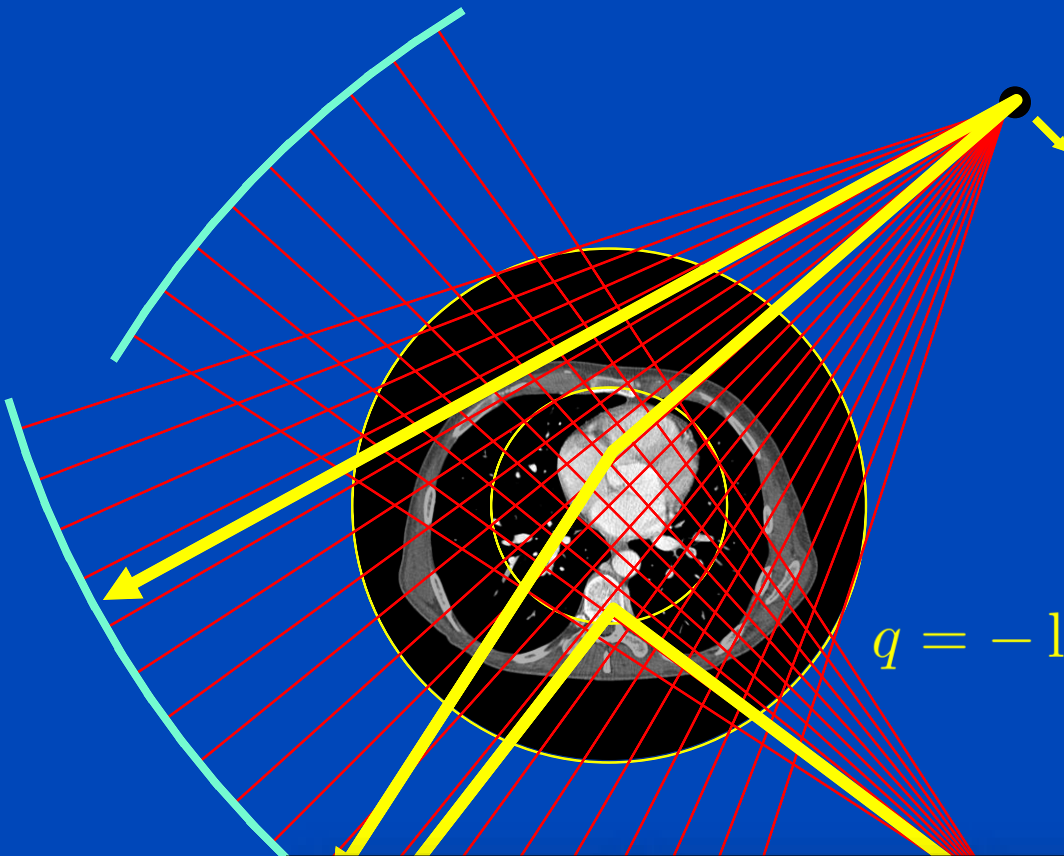

Siemens SOMATOM Force
dual source cone-beam spiral CT

$$q = -\ln \frac{I_{\text{primary}} + S_{\text{forward}} + \rho\, S_{\text{cross}}}{I_0}$$

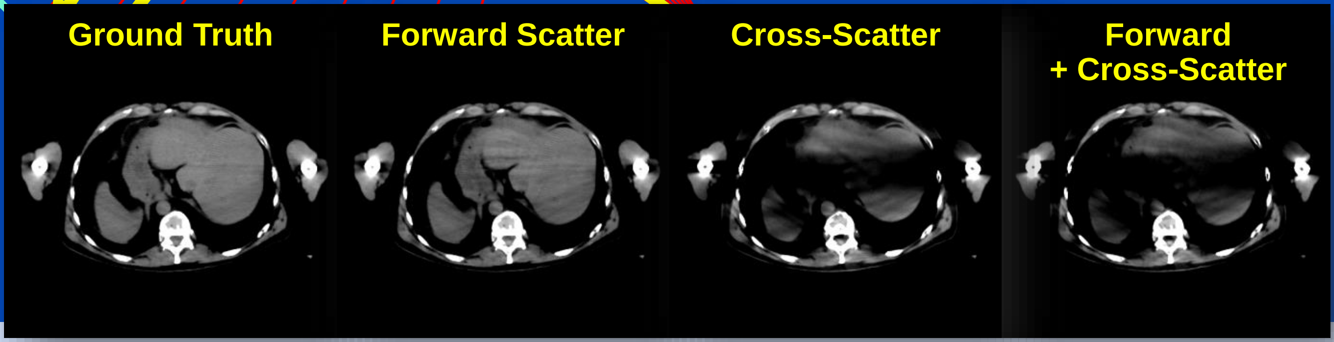

C = 40 HU, *W* = 300 HU, with 2D anti-scatter grid

Measurement-Based Scatter Estimation

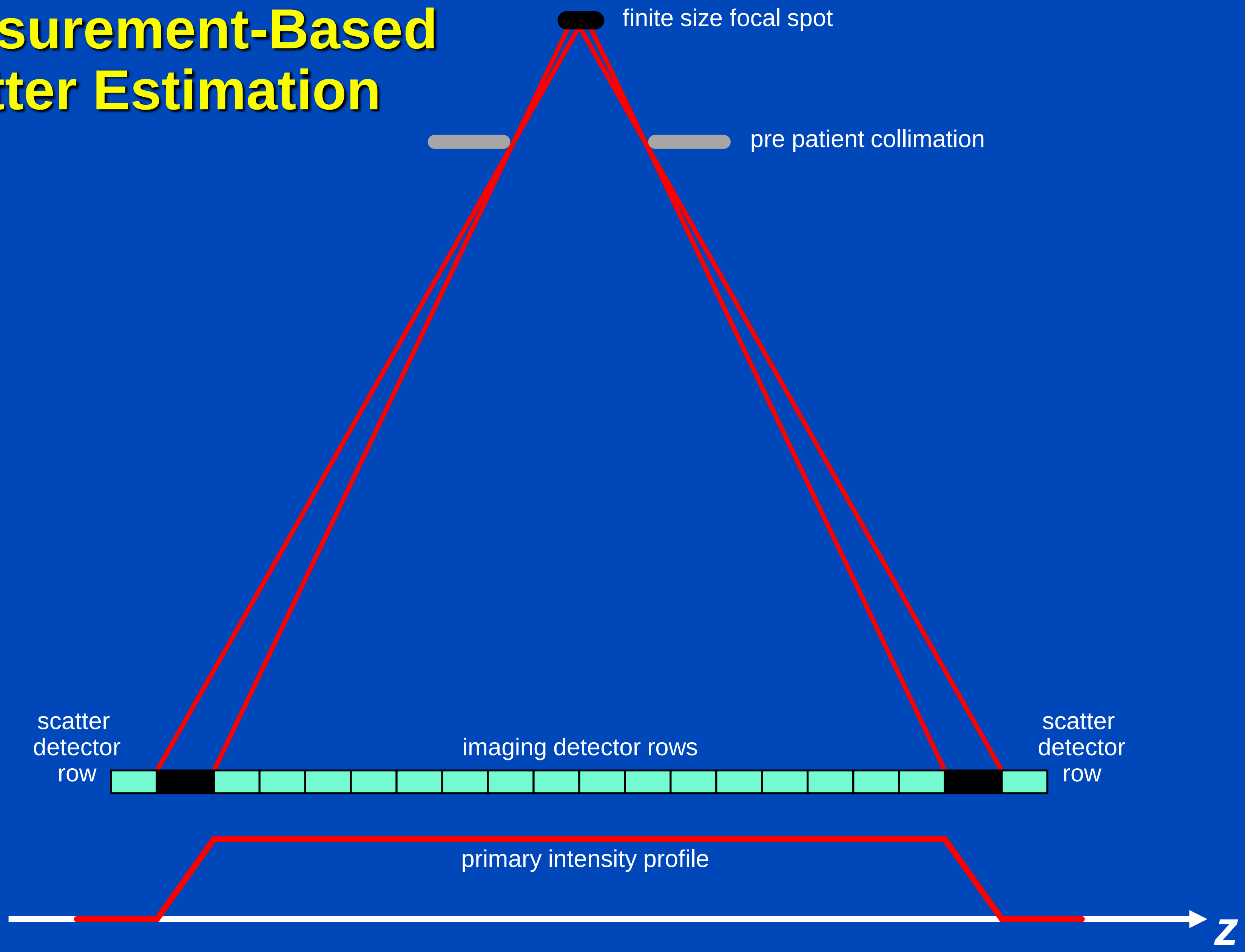

Scatter in Dual Source CT: xDSE

Ground Truth

Uncorrected

xDSE (2D, xSSE)

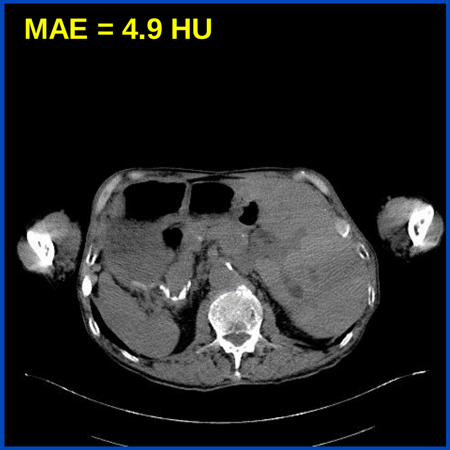

Measurement-based

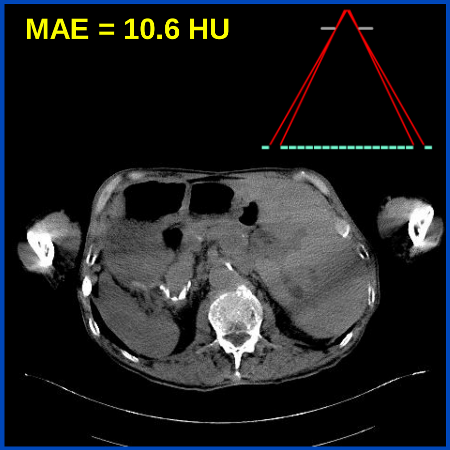

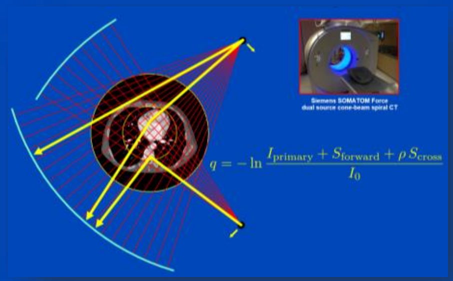

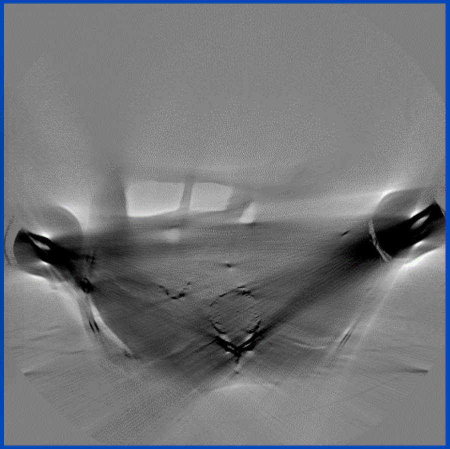

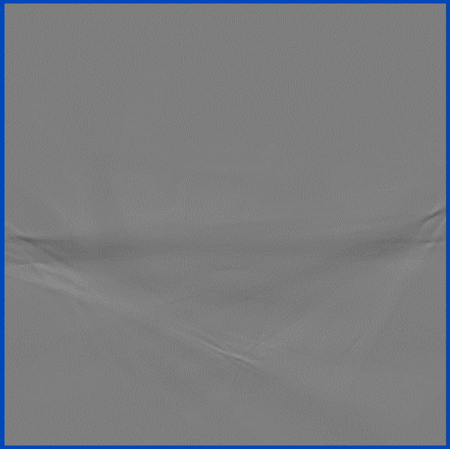

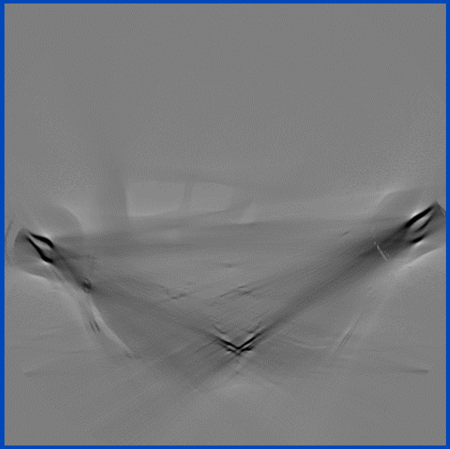

xDSE (2D, xSSE) maps
primary + forward scatter + cross-scatter + cross-scatter approximation → cross-scatter

Images C = 40 HU, W = 300 HU, difference images C = 0 HU, W = 300 HU

J. Erath, M. Kachelrieß et al. Deep learning-based forward and cross-scatter correction in dual source CT. Med. Phys. 48:4824-4842, July 2021.

Conclusions on DSE

- DSE needs about 3 ms per CT projection (as of 2020).
- DSE is a fast and accurate alternative to MC simulations.
- DSE outperforms other approaches.
- Facts:
  - DSE can estimate scatter from a single (!) x-ray image.
  - DSE can accurately estimate scatter from a primary+scatter image.
  - DSE generalizes to all anatomical regions.
  - DSE works for geometries and beam qualities differing from training.
  - DSE may outperform MC even though DSE is trained with MC.
- DSE is not restricted to reproducing MC scatter estimates. It can be trained with any other scatter estimate, including those based on measurements.

J. Maier, M. Kachelrieß et al. Deep scatter estimation (DSE). SPIE 2017 and Journal of Nondestructive Evaluation 37:57, July 2018.
J. Maier, M. Kachelrieß et al. Robustness of DSE. Med. Phys. 46(1):238-249, January 2019.

Deep Cardiac Motion Compensation

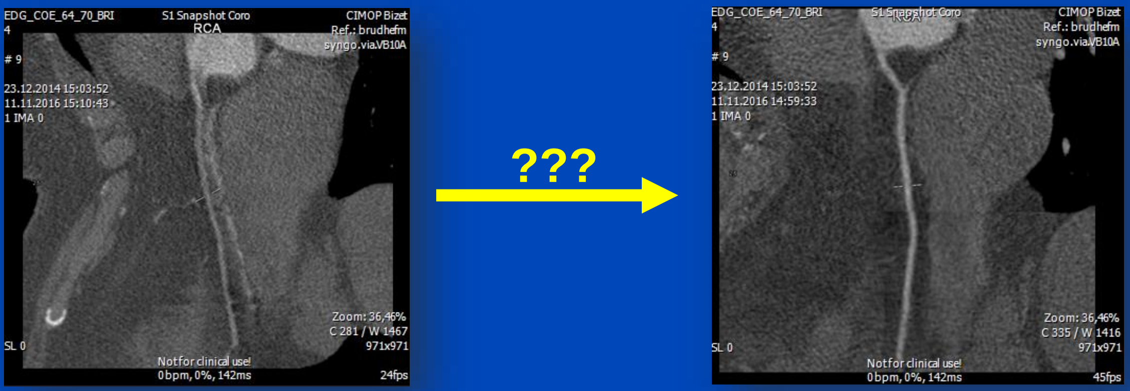

PAMoCo

Generate 2K+1 Partial Angle Reconstructions

Initial segmented stack volume

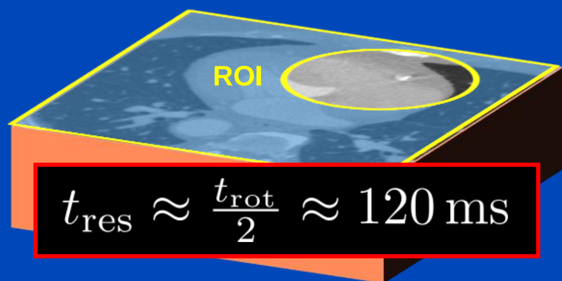

$$t_{\mathrm{res}} \approx \frac{t_{\mathrm{rot}}}{2} \approx 120\,\mathrm{ms}$$

Subdivide the projection data $p'(\vartheta,\xi)$ into 2K + 1 overlapping sectors

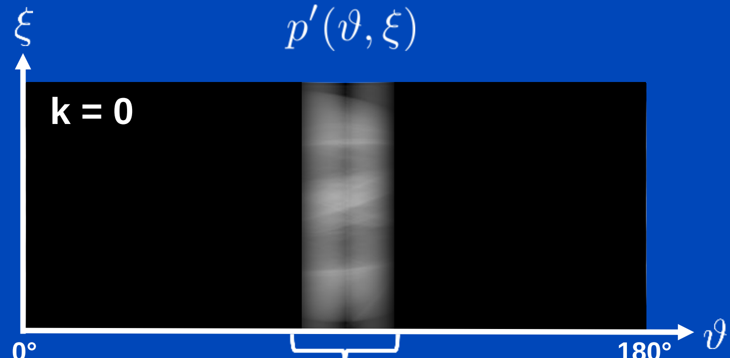

$$p_k(\vartheta,\xi) = w_k(\vartheta)p'(\vartheta,\xi)$$

$$w_k(\vartheta) = \Lambda((\vartheta - \vartheta_k)/2\Delta\vartheta)$$

Partial angle reconstructions $f_k(\boldsymbol{r})$

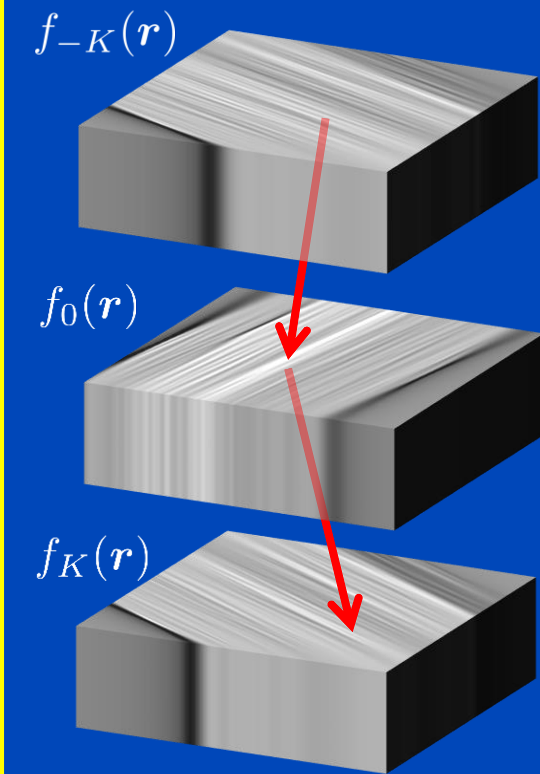

$$t_{\mathrm{res}} \approx \frac{t_{\mathrm{rot}}/2}{(2K+1)/2} \approx 10\,\mathrm{ms}$$

FWHM = $\Delta\vartheta$ **K = 12**

Deep PAMoCo

Network architecture

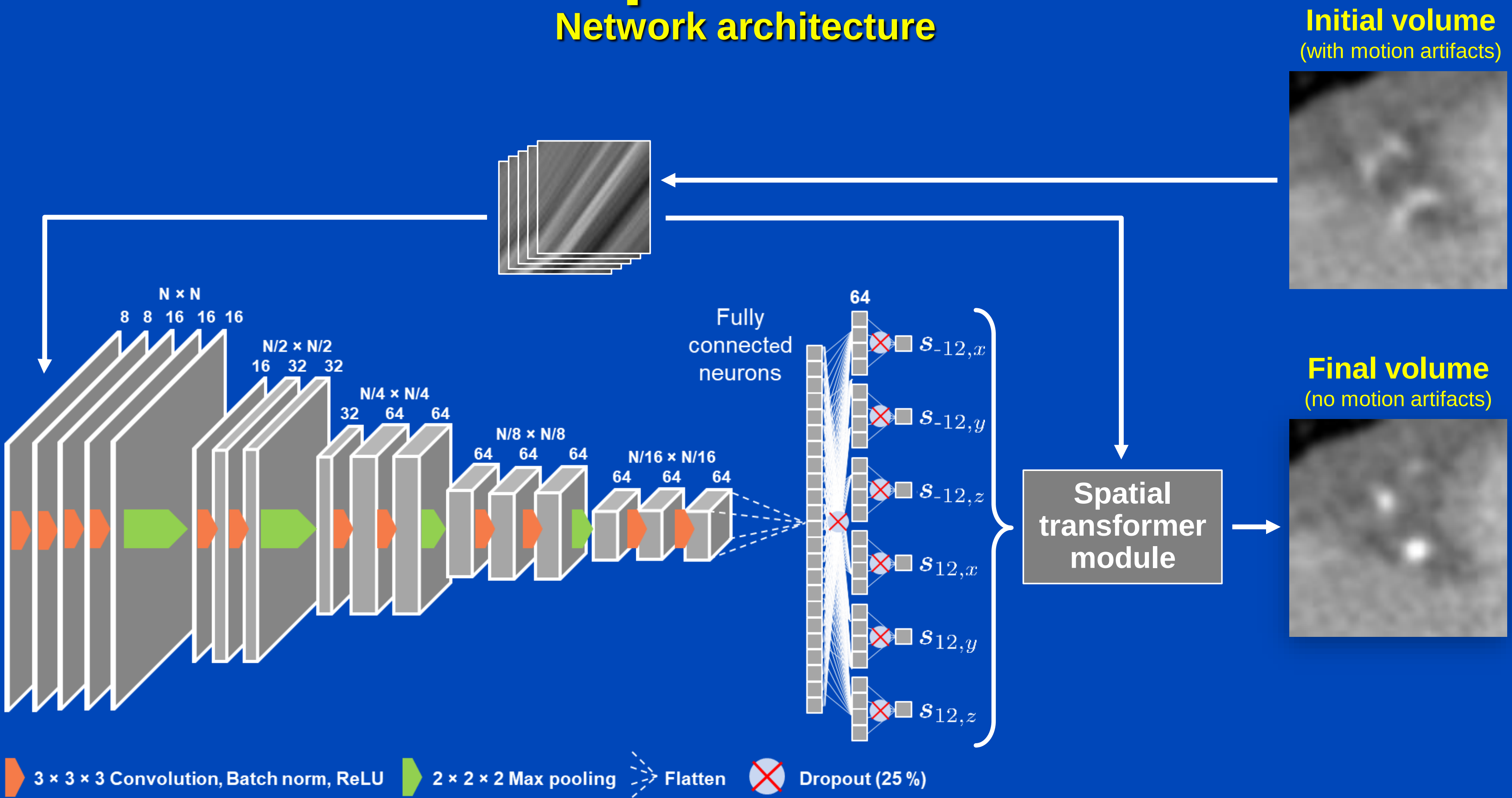

FCN-Layer output: two control points for a cubic spline: for $k = -K$, and for $k = +K$. The third control point at $k = 0$ is (0, 0, 0), i.e. no deformation for the central PAR.

J. Maier, S. Lebedev, J. Erath, E. Eulig, S. Sawall, E. Fournié, K. Stierstorfer, M. Lell, and M. Kachelrieß. Deep learning-based coronary artery motion estimation and compensation for short-scan cardiac CT. Med. Phys. 48(7):3559-3571, July 2021.

Results

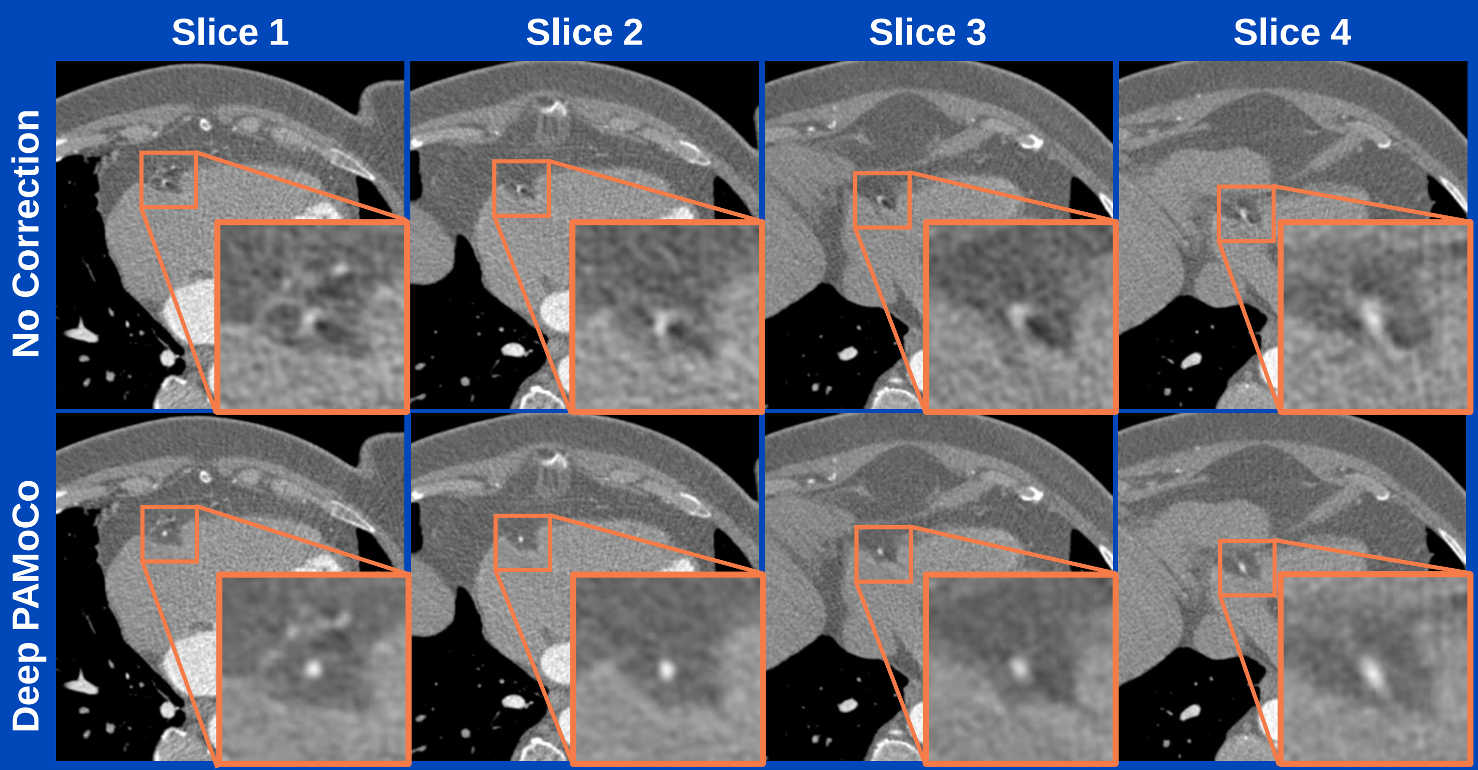

C = 1000 HU
W = 1000 HU

J. Maier, S. Lebedev, J. Erath, E. Eulig, S. Sawall, E. Fournié, K. Stierstorfer, M. Lell, and M. Kachelrieß. Deep learning-based coronary artery motion estimation and compensation for short-scan cardiac CT. Med. Phys. 48(7):3559-3571, July 2021.

Results

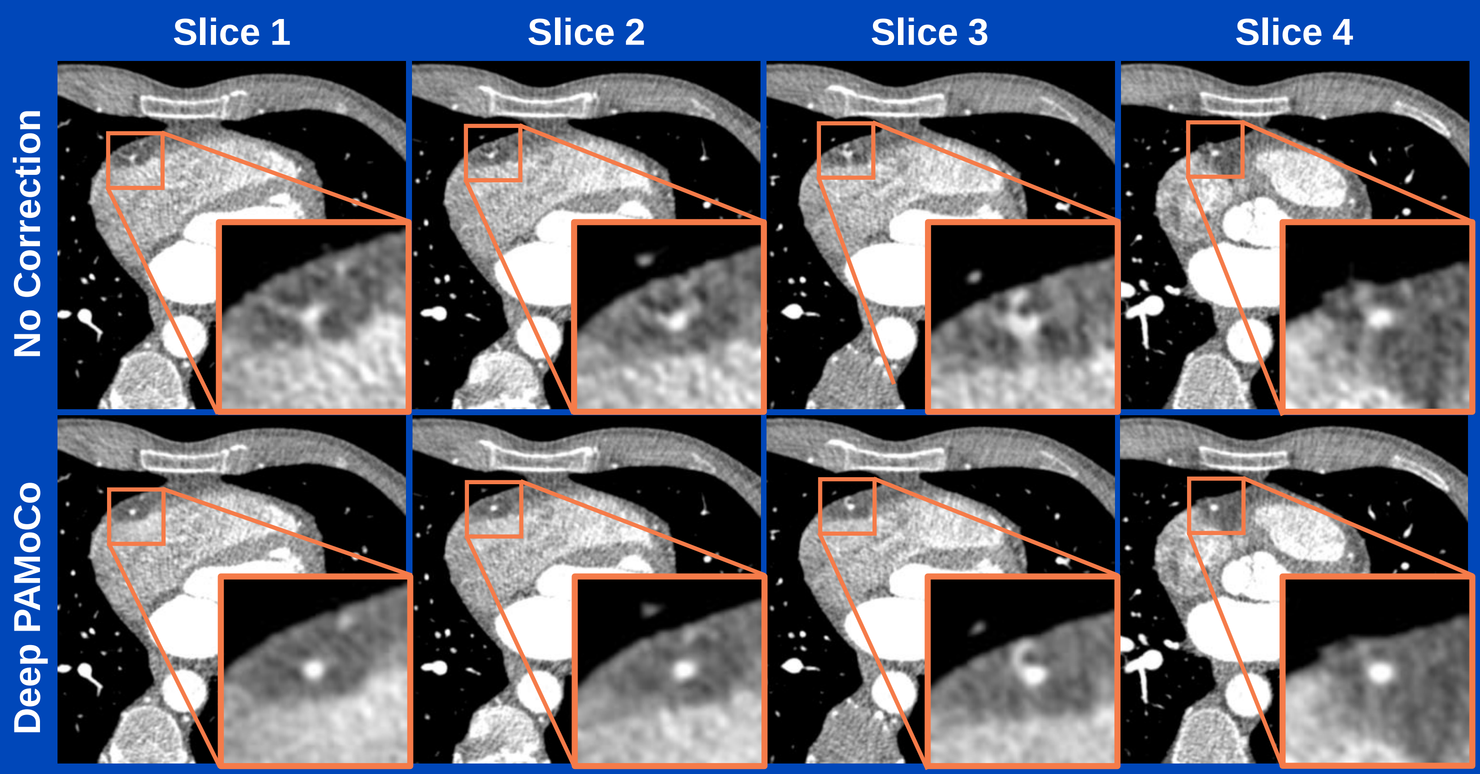

C = 1000 HU
W = 1000 HU

J. Maier, S. Lebedev, J. Erath, E. Eulig, S. Sawall, E. Fournié, K. Stierstorfer, M. Lell, and M. Kachelrieß. Deep learning-based coronary artery motion estimation and compensation for short-scan cardiac CT. Med. Phys. 48(7):3559-3571, July 2021.

Results

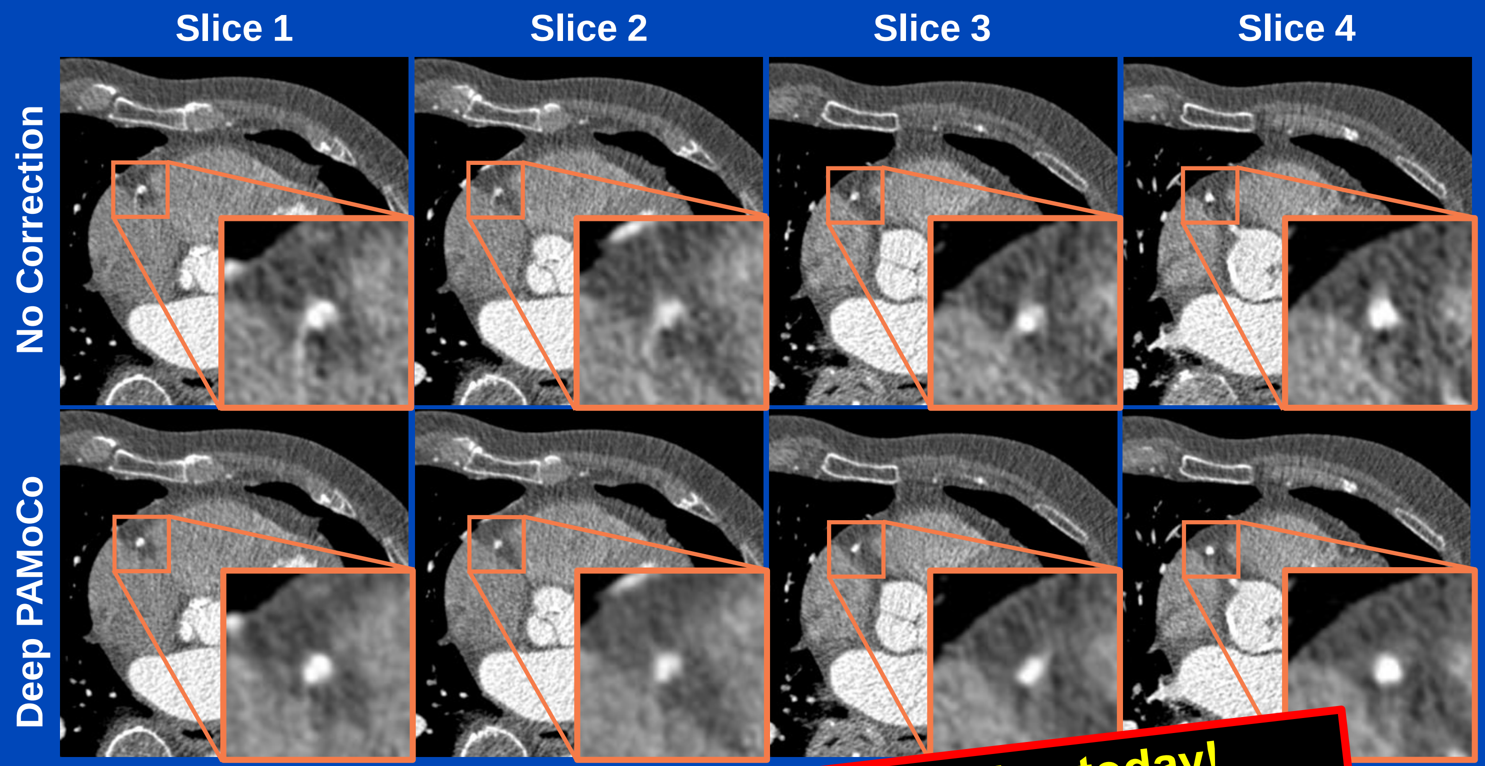

More on Deep PAMoCo upcoming today!

Joscha Maier et al.

Room E351, Session SSPH05, starting 1:30 PM

C = 1100 HU
W = 1000 HU

Are the Methods Reliable?

- Studies about explainability of AI in CT image formation are more than sparse.
- My thoughts:
  - Cosmetic corrections: Unclear if noise reduction, metal artifact reduction etc. is removing/adding lesions. The whole process is a black box.
  - Physical corrections: A clear physical meaning and rawdata fidelity appear more reliable. Examples:
    - » MAR or detruncation networks where the NN output is used only to forward project and inpaint/extrapolate the rawdata
    - » Scatter correction that estimates a smooth physically realistic (trained with MC) scatter signal in intensity domain
    - » Motion correction networks that estimate motion vectors rather than manipulating the voxel values

Thank You!

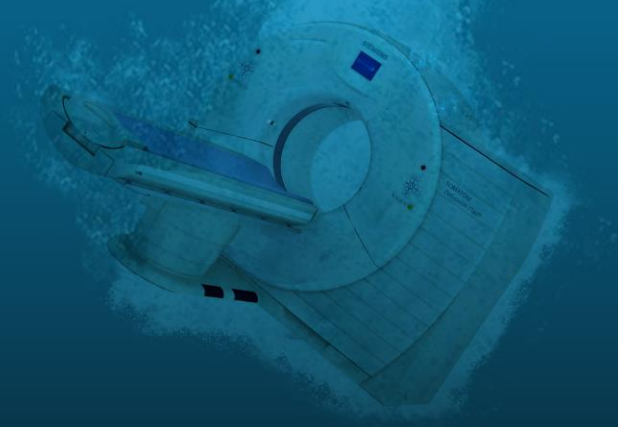

This presentation will soon be available at www.dkfz.de/ct.

Job opportunities through DKFZ’s international PhD or Postdoctoral Fellowship programs (marc.kachelriess@dkfz.de).

Parts of the reconstruction software were provided by RayConStruct® GmbH, Nürnberg, Germany.